

Report

P-21-18

December 2024



Analysis of continuous GNSS measurements in Forsmark 2019–2021

Jan Johansson

SVENSK KÄRNBRÄNSLEHANTERING AB

SWEDISH NUCLEAR FUEL
AND WASTE MANAGEMENT CO

Box 3091, SE-169 03 Solna
Phone +46 8 459 84 00
skb.se

SVENSK KÄRNBRÄNSLEHANTERING

ISSN 1651-4416

SKB P-21-18

ID 1947397

December 2024

Analysis of continuous GNSS measurements in Forsmark 2019–2021

Jan Johansson, RISE Research Institutes of Sweden AB

This report concerns a study which was conducted for Svensk Kärnbränslehantering AB (SKB). The conclusions and viewpoints presented in the report are those of the author. SKB may draw modified conclusions, based on additional literature sources and/or expert opinions.

Data in SKB's database can be changed for different reasons. Minor changes in SKB's database will not necessarily result in a revised report. Data revisions may also be presented as supplements, available at www.skb.se.

This report is published on www.skb.se

© 2024 Svensk Kärnbränslehantering AB

Contents

1	Introduction	5
1.1	GNSS stations used	6
1.2	GNSS data and observation equations	8
1.2.1	Satellite-based errors	8
1.2.2	Errors due to the receiving system and its environment	9
1.2.3	Atmospheric Errors and mitigation	9
1.2.4	Ionospheric Propagation Path Delay	9
1.2.5	Tropospheric Propagation Path Delay	10
1.2.6	Phase Ambiguities	11
1.2.7	Geophysical models	11
2	Method	13
2.1	Precise point positioning	13
2.1.1	Atmospheric effects	13
2.1.2	Antenna offsets	13
2.1.3	Geophysical displacements	13
2.1.4	Differential solution biases	14
2.2	GipsyX – Developed at Caltech and JPL	14
2.3	Analysis methods and Investigation	15
3	Results and Discussion	17
3.1	Station performance	17
3.2	Time Series and Statistical Analysis	18
3.2.1	Kobben (KOB0)	20
3.2.2	Lillkobben (LKB0)	22
3.2.3	Norra Biotesten (NBIO)	24
3.2.4	Söderboda (SOD0)	26
3.2.5	Storskäret (SSK0)	28
3.2.6	Uppsala (UPP0)	30
3.2.7	Västra Måsklinten (VMA0)	32
3.3	Baseline investigation	34
4	Discussion and Conclusions	37
4.1	Recommendations for the future	39
4.1.1	GNSS data analysis software packages and methods	39
4.1.2	GNSS station hardware	39
4.1.3	Recommended further testing	40
	References	41
Appendix	Deliverables and Data formats	43

1 Introduction

The Swedish permanent network of GNSS stations (SWEPOS) operated by Lantmäteriet is under continuous quest for improvements. One area that is particularly important is how the stations with receivers, antennas, radomes, cables, antenna-splitter and pillars/masts are built and linked together. One obvious requirement is that the installations are mechanically stable and do not sway because of wind or temperature changes. Furthermore, it has been found that electromagnetic influences from the environment may interfere with the reception of GNSS signals. Thus, minimizing these effects are essential for further improvement of the robustness and precision in GNSS-methods.

For continuous monitoring of possible ground movements in and around the Forsmark area a total of five GNSS stations have been established. These stations continuously send observation data to Lantmäteriet. Lantmäteriet also process the daily data with the software package developed at the university of Bern in Switzerland. The Bernese Software (Dach et al. 2015) is based on establishing single and double differences between stations pairs and satellite pairs creating a network solution with many stations and all GNSS satellites included. The results reported by Lantmäteriet 2020 indicates a seasonal variation at the level of ± 1 millimeter in the three-dimensional position estimates of the SKB truss mast stations. The possible instability of the truss (or steel grid) masts has been investigated in several earlier studies.

Within an MSc-project in 2010 (Lehner 2011) survey methods to continuously observe local movements of GNSS monuments were developed. Several different monument types were studied in search for both the horizontal and the vertical deformation.

Vertical displacements will in general follow thermal expansion of the mast material. The Lantmäteriet truss mast has, according to Lehner, a thermal expansion coefficient of approximately 7.5 ppm/K, which can be considered small. Temperature variation of up to 40 K in this 3.2 m mast type will lead to variations of the vertical of the mast top of up to 1.0 mm.

Solar heating can cause horizontal variations in the mast top location. The study presented examples of several mm variations due to different expansion in parts of the masts that are solar lit and parts in shadow. This effect motivates the use of lighter monument constructions, such as truss masts, with its relatively high heat dissipation and reduced chance of differential heating; none of the legs are in complete shadow by the rest of the structure. In the study by Lehner the Lantmäteriet mast had horizontal variations within ± 1 mm for the mast top position, see Figure 1-1. It was also noted that the variations could be made smaller by shielding of monument, e.g., with a plastic pipe surrounding the steel grid mast.

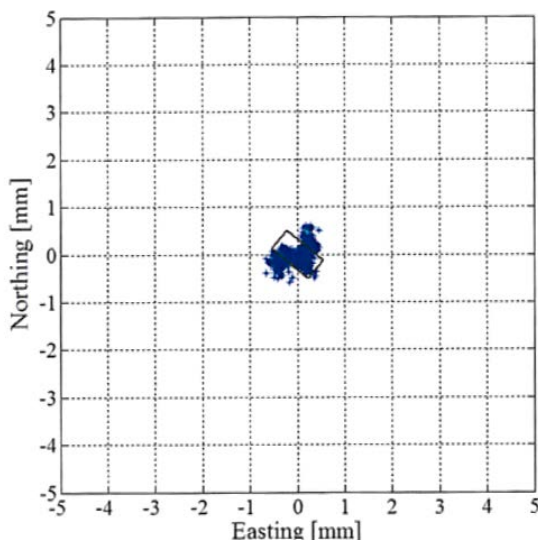


Figure 1-1. The horizontal motion of a Lantmäteriet truss mast top measured using terrestrial optical technique during June 24–28, 2010. From Lehner (2011).

The processing method used by Lantmäteriet is based on double differencing. Single differencing measurements of two receivers to the same satellite eliminates satellite-specific biases; differencing between two satellites and one receiver eliminates receiver-specific biases. As a consequence, double-difference are, to a high degree, free of systematic errors originating from the satellites and from the receivers. Since the atmosphere does not vary much for short baseline lengths, their error contribution to equation is minimal.

The drawback of the double differencing GNSS processing strategies is however that the remaining resulting errors are, most likely a combination of all contributions from any or several of the sites in the network of the stations. Therefore, the error contributions from individual sites are not easily identified. In order to offer an alternative method for analysis of GNSS data from the SKB network, this evaluation is based Precise Point Positioning (PPP) analysis with the GNSS software packages called GipsyX developed by Caltech and Jet Propulsion Laboratory in Pasasadena, USA (Bertiger et al. 2020). PPP (Zumberge et al. 1997) is processing data from only one station at the time, using so called zero baselines, but instead requires high-precision satellite orbits and clocks from the Internal GNSS Service (IGS).

Thus, this report aims to utilize the PPP software GipsyX to study the surrounding environment and local effects around the five GNSS stations included in the network near Forsmark and operated by SKB and Lantmäteriet.

The surrounding antenna environment and local effects are investigated with the help of carrier phase residuals and time series analysis. For some example stations color coded carrier phase residuals are derived. In addition, using a statistical approach where the carrier phase residuals are averaged over both monthly intervals as well as 1° elevation intervals.

Furthermore, we performance time series analysis using tools as Fast Fourier Transform (FFT) and autocorrelation. Finally, we look at interstation baselines in an attempt to identify possible motions in the truss masts or in the ground to which the truss mast is attached i.e., so-called “monument wander”.

1.1 GNSS stations used

The Swedish mapping, cadastral and land registration authority, Lantmäteriet, has a permanent network of more than 500 GNSS stations, SWEPOS with different monumentation such as (i) a concrete pillar station, (ii) a steel grid mast station and (iii) stations mounted on pre-existing buildings (see Figure 1-2 for examples monumentation).



Figure 1-2. Examples of different types of monuments used in the SWEPOS network.

Five of the SWEPOS stations are co-operated by SKB and located near Forsmark (see Figure 1-3). These are all steel grid mast stations.

In this study we use data from the five stations in the SKB-network together with a number of the surrounding SWEPOS stations (<https://swepos.lantmateriet.se/services/mapservice.aspx>). Both the steel grid mast stations and the concrete pillar stations at the fundamental sites are analyzed in the study. In this report we focus on the seven stations listed in Table 1-1. summarized with station ID, location name and horizontal coordinates for each of the steel grid mast stations.

Table 1-1. The seven stations seven used in the study. Five of these are indicated in Figure 1-3.

Station name	Station ID
Kobben	KOB0
Lillkobben	LKB0
Norra Biotesten	NBIO
Söderboda	SOD0
Storskäret	SSK0
Uppsala	UPP0
Västra Måsklinten	VMA0



Figure 1-3. Map of the SKB network of GNSS stations. The reported study used all five stations as well as a number of other SWEPOS stations in the near-field. Especially we here include the station UPP0 (Uppsala) and SOD0 (Söderboda).

1.2 GNSS data and observation equations

Inside each GPS satellite, there are four very precise atomic clocks that provide a few nanoseconds of accuracy. Using these clocks, a fundamental frequency of 10.23 MHz is generated for all communications. The satellites transmit at two or three frequencies, L1 at 1575.42 MHz, L2 at 1227.60 MHz and L5 at 1176.00 MHz. At each of these frequencies, two different codes are transmitted, the Coarse Acquisition (C/A) code with a chip rate of 1.023 MHz and a Precision (P) code at 10.23 MHz. The C/A code is public and is intended for civil usage, while the P code is multiplied with a highly classified code before transmission and its usage is intended for the U.S. military. The other GNSS i.e., GLONASS, Galileo and Beidou also transmit similar signals packages.

The purpose of using several Global Navigation Satellite Systems is to have several satellite constellations operating together to provide better capabilities at the user level. With the availability of multiple satellite constellations, a GNSS receiver would be capable of providing position information even in partially shadowed regions such as urban areas, forests, etc. As the GNSS signals travel from the satellite to the receiver they are affected by several error sources.

There are mainly two types of GNSS measurements used for positioning: the code-based pseudoranges and the carrier-phase measurements. The pseudorange to a satellite j from a receiver station A using code and carrier measurements is given by the two following equations, respectively,

$$P_A^j = \rho_A^j + c\tau_A - c\tau^j + Z_A^j + I_A^j + v_A^j \quad (1-1)$$

$$L_A^j = \rho_A^j + c\tau_A - c\tau^j + Z_A^j - I_A^j + \lambda N_A^j + \eta_A^j \quad (1-2)$$

where P or L is the Pseudorange from code or carrier measurements respectively, ρ is the true range, c the velocity of light, τ^j and τ_A are the satellite and receiver clock errors, Z the tropospheric propagation path error, I the Ionospheric error, λ the wavelength of transmitted signal for L_1 and L_2 frequencies (of GPS), N the bias due to integer cycle ambiguity and v and η are the bias due to various other error sources as mentioned below.

Looking closer at ρ , the true distance between receiver and satellite, it can be written as

$$\rho_A^j = \sqrt{(X^j(t^j) - X_A(t_A))^2 + (Y^j(t^j) - Y_A(t_A))^2 + (Z^j(t^j) - Z_A(t_A))^2} \quad (1-3)$$

where $X^j(t^j)$, $Y^j(t^j)$ and $Z^j(t^j)$ are the satellite coordinates which are broadcast and at meter level uncertainty from the satellites. The satellite clock error, τ^j , is also available in the satellite data message. However, if we want to have millimeter level global positioning, we need to retrieve more accurate satellite orbit and satellite clock information. So the unknown term is the receiver coordinates $X_A(t_A)$, $Y_A(t_A)$ and $Z_A(t_A)$ and the receiver clock error, which need to be solved. Also, the other parameters in Equations (1-2) and (1-3) needs to be handle either with models, accompanied by *a priori* information and/or estimated in the GNSS data analysis.

Errors in the GNSS measurements are broadly classified as: satellite-based errors, propagation medium or atmospheric errors and receiver-based errors. Some errors can be removed, and some can be reduced. Understanding of the significance of these errors is important for applications especially requiring high accuracy measurements.

1.2.1 Satellite-based errors

There are five major types of satellite-based errors. They are: clock errors due to instability of onboard atomic clocks, ephemeris errors due to errors in the estimated satellite positions, instrumental bias due to Radio Frequency (RF) components of satellite and receiver, relativistic effects due to different gravitational potential experienced by satellite and receiver clocks and selective availability (if any) due to intentional degradation of the GNSS (true only for GPS) signal in frequency and time domain. Satellite geometry is also crucial for accurate measurements. In GNSS applications, possible limitations in precision is represented by the term Dilution of Precision (DOP). Poor geometry will lead to a large DOP. Good geometry means that the received satellites are evenly distributed in a geometrical

space. For example, in the case of four satellites, the azimuth angle between each satellite should be 120 degrees complemented by one satellite close to zenith. At high latitudes, as in Sweden, DOP values could be limiting the accuracy of the estimated coordinates. The general overall GNSS design was for unaided code observations and was specified to a global coverage with at least four satellites in view above five degrees elevation at 99.9 % of the time. Today, with all available GNSS, there are more than 20 satellites visible at any given location and time. Still there might be geometry issues related to high DOP in areas with high horizon masks (cities, forests, mountain, mines etc).

The errors of the broadcast satellite orbital parameters are about 0.3–2 meters depending on the GNSS (Galileo is the best). Similarly, errors in satellite clocks, converted to distance using the velocity of the waves, are about 0.2–1 meter.

Many GNSS data analysis software packages, such as the Bernese Software, utilizes differential methods to remove or at least minimize the effect of satellite orbits and clocks errors in the analysis.

When instead using a software package like GipsyX, based in the Precise Point Positioning method, double differencing is not used. Thus, improved satellite orbits and clocks are necessary in order to achieve millimeter-level results. Such high-quality GNSS satellites orbits and clocks are available from the International GNSS Service (IGS). IGS analysis centers uses data from a global network of stations in order to produce daily satellite orbit and clock products accurate to the level of at ± 2 centimeters in global reference frame.

1.2.2 Errors due to the receiving system and its environment

There are five types of major receiver-based errors. They are receiver noise and resolution due to limitations of receiver electronics, receiver clock error due to use of inexpensive crystal clocks, which are less accurate than that of GNSS satellite clock, instrumental bias due to RF components of receiver, Multipath due to interference caused by reflected signals arriving at the receiver and antenna phase centre variation due to various antenna types that are used for receiving GPS signals. Antenna phase centre for a receiver varies with frequency, elevation and azimuth and is therefore quite difficult to model. The code Multipath errors for each satellite for successive days can be isolated by calculating the Code-Minus-Carrier values. Multipath error repeats itself with each passing sidereal day if the environment around the antenna remains the same for successive days. Effective signal processing using adaptive filters for two successive days can extract out multipath. The calculated Multipath error is smoothed with Carrier smoothing filter to remove the high frequency receiver noise.

1.2.3 Atmospheric Errors and mitigation

The satellite signals, broadcasted from GNSS satellites 20 000 km above Earth surface, propagate through atmospheric layers as they travel from the satellite to the receiver. Two layers are generally considered when dealing with GPS: the ionosphere, which extends from a height of about 50 to 1 000 km above the Earth, and the troposphere which stretches to about 16 kms above the equator and 9 kilometres above the poles from the surface of the earth.

1.2.4 Ionospheric Propagation Path Delay

The ionosphere is a region of ionized gases (free electrons and ions). The principal source of ionization in the ionosphere is the electromagnetic radiation from the sun. As the GPS signal travels from the satellite to the receiver, the presence of free electrons in the ionosphere changes the velocity (speed and direction) of propagation of the signals. The change in signal speed changes the travel time of the signal, and therefore the apparent range to the satellite. The ionosphere is not uniform in composition, and the refractive index changes all along the path of a signal. The effect of signal bending causes a range error, which is quite substantial at very low elevation angles less than 5° . The ionosphere speeds up the propagation of the carrier phase beyond the speed of light, while it slows down the C/A code (and the navigation message) by the same amount. Therefore, the receiver-satellite distance will be too short if measured by the carrier phase and too long if measured by the code, as compared with the actual distance. The ionospheric delay is proportional to the number of free electrons along the propagation path, which is known as the Total Electron Content (TEC). Further, this delay is dependent

on three main factors: the geomagnetic latitude of the receiver, the time of day and the elevation of the satellite. A technique to remove a large part of the contribution from the ionosphere is to form a linear combination, L_3 , of the L_1 and L_2 observables. We know that the propagation path delay in the Ionosphere can be written as a function of (TEC) and frequency

$$\Delta L = \frac{40.3}{f^2} TEC \quad (1-4)$$

The carrier phase observables of each frequency with Ionosphere delay can be written as observations without Ionosphere delay L_t plus the difference ΔL :

$$L_1 = L_t + \Delta L_1 \quad (1-5)$$

$$L_2 = L_t + \Delta L_2 \quad (1-6)$$

From the two equations above, we can derive L_t as follows:

$$L_t = L_1 - \Delta L_1 = \frac{40.3}{f_1^2} TEC \quad (1-7)$$

$$L_t = L_2 - \Delta L_2 = \frac{40.3}{f_2^2} TEC \quad (1-8)$$

$$L_3 = L_t = \frac{f_1^2}{f_1^2 - f_2^2} L_1 - \frac{f_2^2}{f_1^2 - f_2^2} L_2 \quad (1-9)$$

L_3 is a new observable without Ionosphere. We know for GPS the two carrier frequencies are $f_1 = 1575$ MHz and $f_2 = 1227$ MHz. By inserting these two values, we can get the final equation and the same for code measurements.

$$L_3 = 2.546 L_1 - 1.546 L_2 \quad (1-10)$$

$$P_3 = 2.546 P_1 - 1.546 P_2 \quad (1-11)$$

This method removes most of the ionospheric propagation path delay while the noise level is increased by a factor of 3 compared to the noise level of L_1 and L_2 , respectively. The Equations (1-10) and (11) is specific for GPS while Equation (1-9) is general where the frequencies of the other GNSS, with slightly different frequencies, can be inserted.

1.2.5 Tropospheric Propagation Path Delay

The troposphere is the lower part of the atmosphere that is non-dispersive for frequencies up to 15 GHz. The troposphere causes a delay in both the code and carrier observations. Since it is not frequency dependent (within the GNSS frequency range 1 100–1 600 MHz) it cannot be canceled out by using dual frequency measurements, but it can, however, be successfully modeled accurately. The troposphere can be split into two parts: the dry component, which constitutes about 90 % of the total refraction, and the wet part, which constitutes the remaining 10 %. Values for temperature, pressure and relative humidity are required to model the vertical delay due to the wet and dry part, along with the satellite elevation angle, which is used with an obliquity/mapping function.

The Tropospheric error is computed by calculating a product of the ZTD (the Zenith Tropospheric Delay) with $m(\varepsilon)$ (the mapping function). However, no external observations or data are accurate enough to be used in the data processing for high-accuracy applications. Instead, ZTD is estimated in our Kalman filter-based software, GipsyX, using a random walk process. A similar approach is used also in other high-level GNSS software packages such as the Bernese Software.

1.2.6 Phase Ambiguities

The big challenge using carrier phase measurement is how to accurately determine/estimate the number of cycles N . There is only one phase ambiguity term per satellite per satellite passage. So, if we have 24 hours observations, each satellite in the GPS constellation will pass over us twice per 24 hours. That means if we have 32 satellites passing by twice every day, there will be 64 phase ambiguity terms solved as constant. In our software, GipsyX, we will estimate (correct for) N as an unknown parameter.

1.2.7 Geophysical models

In geodesy, earth orientation parameters (EOP) illustrate irregularities in the rotation of planet Earth. EOP provides the rotational transform from the International Terrestrial Reference System (ITRS) to the International Celestial Reference System (ICRS), or vice versa, as a function of time. Earth tide is the displacement of the earth's surface from the influence of the Sun and the Moon's gravitational forces. Displacements caused by ocean tidal loading can exceed the displacements due to the Earth's body tide. Internationally agreed models for reference frames, EOP, Earth tides, and ocean tides are implemented in all high-precision geodetic software packages. These models are constantly revised and update by the *International Earth Rotation and Reference System Service (IERS)*. Software packages like the Bernese Software and GipsyX have the same and latest IERS models implemented.

2 Method

2.1 Precise point positioning

Precise point positioning (PPP) is a technique where accurate data about the satellite orbits and clocks are needed. Since the accuracy of the broadcast orbit information is at meter-level this study, as all high-precision GNSS applications, utilizes final orbit and clock products from the International GNSS service (IGS) which has uncertainties on the order of 1–2 cm. The orbit and clock products are calculated at the IGS analysis center. The final products can only be used for post-processing, since they have a latency of approximately 14 days.

In order to achieve a millimeter precision, GipsyX utilizes several other error correction products as well. The products used can be divided in: (i) atmospheric effects, (ii) antenna offsets, (iii) geophysical displacements and (iv) differential solution biases.

2.1.1 Atmospheric effects

GipsyX utilizes products from two different sources for the tropospheric and the ionospheric path delay. The products that model the second order ionospheric effects are downloaded from the IGS analysis centers. For the tropospheric path delay GipsyX utilizes the Vienna mapping function (VMF), which is downloaded from TU Wien.

2.1.2 Antenna offsets

The antenna phase center (APC) has an offset relative to the antenna reference point (ARP). GipsyX utilizes antenna calibration files from IGS that models these offsets for both the receiver and the satellites' and they are named `igs14_2114.xyz` and `igs14_2114.atx`, respectively. There is a second offset that relates to the satellites that GipsyX also accounts for. The precise orbits from IGS refers to the satellites' center of mass and in order to refer the measurements to the ARP, GipsyX utilizes a correction file from IGS, named `igs14_2114.pcm`, that models the center of mass offset.

2.1.3 Geophysical displacements

There are three different geophysical tidal effects that are taken into account by GipsyX: (i) solid tides, (ii) ocean tides and (iii) polar motion. The station coordinates will be analyzed as constants over 24-hour periods in the study and the geophysical models are needed because the station experiences daily displacements that needs to be accounted for.

The solid tides relate to the movement of Earth's crust that is caused by the gravitational forces of the sun and the moon, primarily. It is compensated in GipsyX with products from the International Earth Rotation and Reference Systems Service (IERS).

The same gravitational forces that cause the solid tides also affects the oceans. When the oceans deform the underlying sea floor, the adjacent land area is also Displaced. Its effect is accounted for in GipsyX with the ocean tide loading model FES2004. The model coefficients depend on the station coordinates so each station has its own specific model and they are downloaded from.

The Earth's axis of rotation has an offset as compared to the geophysical axis that varies periodically. This phenomenon is what is called polar motion. The polar motion together with the difference in the satellites' time scale, UT1-UTC is monitored by IERS and their combined product is called Earth Orientation Parameters (EOP). The EOP are used together with the Earth Rotation Parameters (ERP), that are provided by IGS, to transform between the celestial and the terrestrial reference frames.

2.1.4 Differential solution biases

The first order ionospheric effects are removed in PPP, and in GipsyX, with the ionospheric free models P_3 and L_3 for the code and carrier phase pseudoranges. The forming of L_3 introduces a third carrier phase ambiguity that has to be solved for in the PPP processing. GipsyX utilizes products calculated by the IGS analysis centers that enables faster convergence times for the new carrier phase ambiguity and they are called wide-lane phase bias (WLPB) products.

2.2 GipsyX – Developed at Caltech and JPL

The GipsyX software, often run in a PPP mode, is developed by NASA’s Jet Propulsion Laboratory. It is a complete redesign of their former version GIPSY-OASIS, where GIPSY stands for GPS Inferred Positioning System and OASIS stands for Orbit Analysis Simulation Software (Zumberge et al. 1997 and Bertiger et al. 2020). The latest version, GipsyX 2.0, can process all four GNSS constellations both in real-time and post-processing. A simplified block schematic of the different processing steps in GipsyX is illustrated in Figure 2-1.

The different boxes in Figure 2-1 are numbered to simplify the explanation of their respective functionalities and they will be described by their respective box numbers. In box 1, the GipsyX software utilizes RINEX observation files from the SWEPOS stations as input.

In box 2 of Figure 2-1, GipsyX performs editing of the data. It removes data that does not help the solution, i.e., outliers that are above or below a certain threshold. If a receiver loses track of a satellite and it consequently leads to too short periods of data availability, GipsyX removes those periods as well. When the editing is performed, it creates the ionospheric free model, for the code (P_3) and the carrier phase (L_3) measurement.

In box 3 of Figure 2-1, information is collected from the external sources, as was described in Section 2.1. The precise final products for the satellites’ orbits and clocks are downloaded from the IGS, together with the other products needed to reach sub-centimeter precision. The second source of external information comes from IERS which provides information about the solid tides and the EOP.

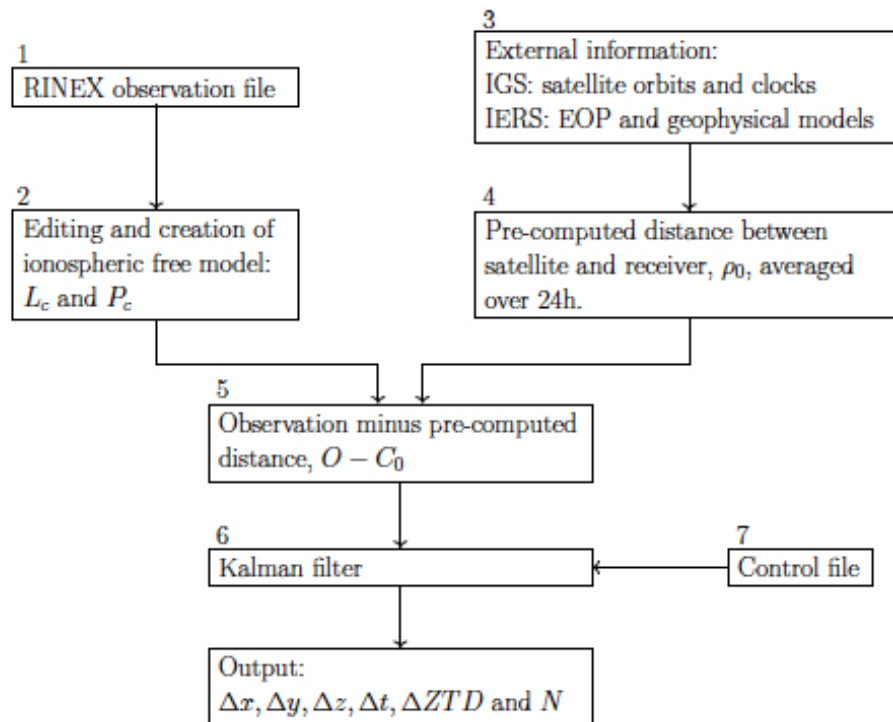


Figure 2-1. Block schematic of the GipsyX processing steps using the PPP strategy.

In box 4, GipsyX performs a pre-computed distance between the satellites and the receiver. In order to do that, GipsyX requires initial values for six parameters, which are listed in Table 2-1 (the same six parameters is also the final output of the Kalman filter). These starting values can be regarded as the initial guess of the parameter values e.g., the initial guess of coordinates can be based on an assumed station position within ± 100 meters from the true position in the global reference frame.

Table 2-1. A priori values of the coordinates (x_0 y_0 z_0), receiver clock (Δt_0), the zenith tropospheric delay (ZTD_0) and phase ambiguities (N) for all the estimated parameters in the PPP processing with the GipsyX software.

Parameter	Value
x_0, y_0, z_0	Taken from the RINEX header
Δt_0	The receiver clock error is unknown, so it's set to 0 s
ZTD_0	The zenith tropospheric delay could e.g. be 2.3 m
N	The phase ambiguity is unknown, so it's set to 0 s

In box 5, GipsyX subtracts the pre-computed distance, C_0 , from that of the ionospheric free model of the observations, O . This is done for both the code and the carrier phase measurement and the result are used as input to the Kalman filter. The parameters that the Kalman filter estimates is controlled by the control file. It controls how often each parameter is supposed to be estimated and what kinds of noise parameters there are. Table 2-2 lists the update intervals and the motivations for each of the six parameters.

Table 2-2. Parameter estimation intervals in the KF and their motivations.

Parameter	Value
$\Delta x, \Delta y, \Delta z$	Solve as constants over 24 h. This removes the daily variations and it implies that the geophysical models from IERS are reliable
Δt	Solve every 300 s epoch. Δt is modeled as a white noise parameter, since it varies a lot as compared to the satellites' atomic clocks
ΔZTD	Solve every 300 s epoch. This is because the ZWD has a relatively fast variation. Modeled as a random walk parameter
N	Solve as a constant with wide-lane phase bias products from IGS. When the receiver starts tracking, N remains the same until it loses its tracking

The Kalman filter can use any of the four GNSS systems separately as well as combining any of them in the solution process and it is also controlled by the control file. The control file furthermore controls the maximum iterations that the Kalman filter can perform before the final output is produced.

2.3 Analysis methods and Investigation

Section 1 described the 5 GNSS stations in the SKB network investigated. The PPP solutions for these steel grid mast stations are analyzed with respect to: (i) repeatability for the four GNSS constellations, (ii) sky plots with color coded post-fit carrier phase residuals for GPS and Galileo and (iii) monthly mean post-fit carrier phase residuals for GPS and Galileo.

It is common in GNSS terminology to abbreviate GPS, GLONASS, Galileo and BeiDou as G, R, E and C, respectively. The coordinate repeatability for the six steel grid masts and one concrete pillar stations are analyzed for the constellation combinations G, R, E, C, GE, GR, GRE and GREC. The standard deviation is used as the measure for the repeatability throughout the result presentation.

The solution interval for the receiver clock error as well as the ZTD in the Kalman filter (KF) in GipsyX is set to 300 seconds. The choice of 300 seconds builds on experience from the BIFROST project (Johansson et al. 2002, Lidberg et al. 2007, Kierulf et al. 2021). Even if the RINEX files

provided by the SKB station contains data with sample interval of 30 seconds is appropriate to decimate the use of the data to 300 seconds without losing quality but saving processing time. Decades of experience from the daily analysis of all permanent GNSS stations in north Europe show that this decimation procedure does not impact on the coordinate results. Using all data in the raw data file will not change the actual values of the parameter but still result in lower uncertainties. This is however an illusion since GNSS data have strong temporal correlation.

The KF produces one post-fit carrier phase residual per visible satellite per 300-second period and the post-fit carrier phase residual is the difference between the observation, i.e., the actual measurement, and the computed output. The KF also produces post-fit residuals for the code-based solutions but those will not be used in the study. The post-fit carrier phase residuals are one of the main analysis methods in the study and they will henceforth be called residuals, for simplicity.

The residuals are used to examine the local environment around the antenna as well as systematic effects that affects all of the stations. The residuals are presented using sky plots with color residuals as well as using a statistical approach where the residuals are averaged over both monthly intervals as well as 1° elevation intervals.

The sky plots illustrate the residuals as a function of both azimuth and elevation and they are thus a useful tool to examine the local effects around the stations. It is for instance possible to discern if the residuals are higher in any direction which might indicate that there is more multipath in that direction.

The statistical approach where the residuals are averaged over both monthly intervals as well as 1° elevation intervals is useful to study the overall behavior of the station. However, the monthly mean has no azimuth dependence, since it is visualized as a function of elevation angle, which is why it might be useful to analyze it in parallel with the sky plots. The sky plots and monthly mean residuals for three of the seven stations are presented in Section 3.1.

3 Results and Discussion

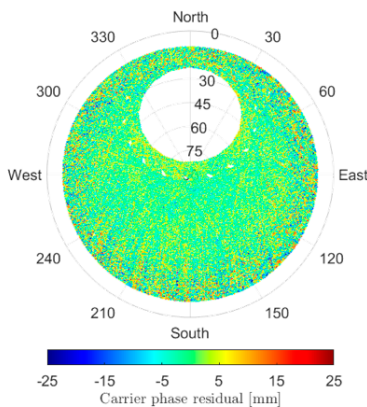
3.1 Station performance

As mentioned in Section 2.3, the post fit residuals could be examined in order to investigate the quality of a GNSS station. In Figure 3-1 through 3.3 the post fit residuals for three of the GNSS stations are plotted in accordance to the method described in Section 2.3. The residuals are visualized in sky plots or residual plots as a function of the elevation of the satellite at the epoch of observation. If the local multipath environment surrounding the station is good, we should see only small residual variations as a function of elevation and azimuth. The residual analysis is performed for all SWEPOS and SKB stations but only three stations are reported here. The rather unique station Storskåret (SSK0) having a very high steel grid mast, is shown in Figure 3-1. The more traditional monument at Kobben (KOB0) is shown in Figure 3-2. Finally, the SWEPOS station Uppsala (UPP0) established with the original three-meter concrete pillar is shown in Figure 3-3. Clearly, post fit residuals with systematic behavior as a function of elevation angle is found for the station Uppsala (UPP0), equipped with a SWEPOS concrete pillar monument, while the two SKB stations, both equipped with truss masts, seem to have an excellent multipath environment. Since all other SKB stations have the same high-quality local environment, these plots are not included. This also verifies the fact that the GNSS data provided by all SKB stations are of high quality and very few observations have had to be removed in the data processing.

The steel grid mast stations in SWEPOS seem to have a slightly better multipath environment (even if the concrete monuments have other advantages). Thus, all SKB stations show very low influence from multipath and the receiving systems in the SKB network are state-of-the-art.

One possible problem with the SKB station that could be investigated further is the risk of occasional variations in reflections/multipath patterns caused by changes in ocean surface (sea level and waves).

Skyplot, GPS, GLONASS and Galileo, SSK0, 300s data rate
Period: 2018-12-01 - 2021-03-06



Carrier phase residual, 1° interval, SSK0
Period: 2018-12-01 - 2021-06-30

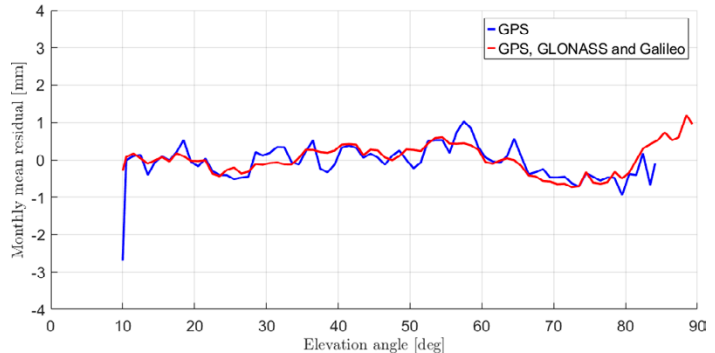
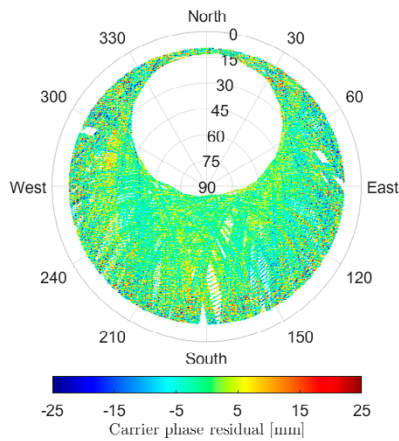


Figure 3-1. Post fit residual for the station Storskåret (SSK0) visualized as a sky plot (left) and residuals as a function of elevation (right). SSK0 is a steel grid mast of a different kind than the standard SWEPOS monumentation shown in Figure 1-2. The SSK0 steel grid mast is about 10 meters and surrounded by forest and vegetated land.

Skyplot, GPS, no-fiducial, KOB0, 300s data rate
 Period: 2018-12-01 - 2021-06-30



Carrier phase residual, 1° interval, KOB0
 Period: 2018-12-01 - 2021-06-30

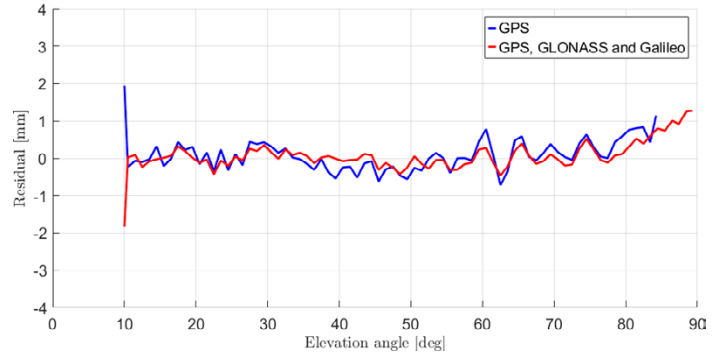
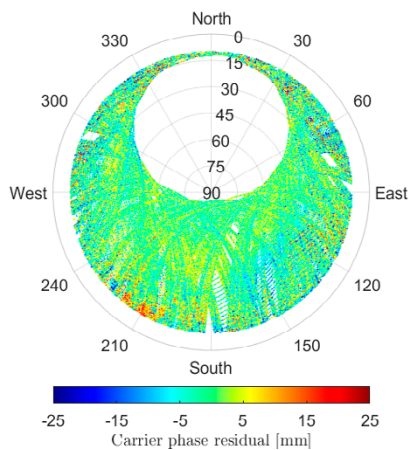


Figure 3-2. Post fit residual for the station Kobben (KOB0) visualized as a sky plot (left) and residuals as a function of elevation (right). KOB0 has a standard SWEPOS steel grid mast monument shown in Figure 1-2 and surrounded by bedrock.

Skyplot, GPS, no-fiducial, UPP0, 300s data rate
 Period: 2018-12-01 - 2021-06-30



Carrier phase residual, 1° interval, UPP0
 Period: 2018-12-01 - 2021-06-30

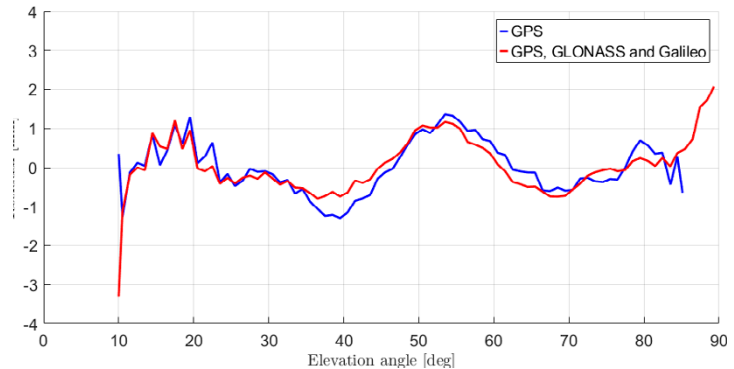


Figure 3-3. Post fit residual for the station Uppsala (UPP0) visualized as a sky plot (left) and residuals as a function of elevation (right). UPP0 has the original SWEPOS concrete 3-meter pillar shown in Figure 1-2. The station is surrounded by partly vegetated bedrock. The residual pattern as a function of elevation is typical for the concrete pillar stations in SWEPOS.

3.2 Time Series and Statistical Analysis

Table 3-1 summarizes the results in terms of linear regressions of the three-year time series from the seven focus stations. The analysis has been performed in the International Terrestrial Reference Frame (ITRF) 2014. The results are very homogeneous in terms of both the three-dimensional velocities, as well as the uncertainty of these velocities. This comes as no surprise when looking at the unsurpassed data quality from the SKB network. As noted in Section 3.1, the multipath footprint at the SKB stations is very low and the post fit residuals are flat. Also, the number of deleted observations in the processing are very low in comparison to the SWEPOS core stations.

Table 3-1. Estimated three-dimensional station velocities and their respective uncertainties based on a linear regression on three years of daily observational data from seven stations around Forsmark.

Station name	Station ID	Latitude velocity and uncertainty (mm/y)	Longitude velocity and uncertainty (mm/y)	Height velocity and uncertainty (mm/y)
Kobben	KOB0	13.71 ± 0.06	18.75 ± 0.06	6.25 ± 0.22
Lillkobben	LKB0	13.61 ± 0.06	18.52 ± 0.07	6.16 ± 0.23
Norra Biotesten	NBIO	13.73 ± 0.06	18.68 ± 0.07	6.36 ± 0.23
Söderboda	SOD0	13.72 ± 0.06	19.14 ± 0.07	6.75 ± 0.23
Storskäret	SSK0	13.72 ± 0.06	18.84 ± 0.07	6.37 ± 0.23
Uppsala	UPP0	13.68 ± 0.06	18.75 ± 0.07	5.75 ± 0.22
Västra Måsklinten	VMA0	13.57 ± 0.06	18.57 ± 0.07	6.17 ± 0.24

In following subsection, we report on each individual station in Table 3-1. The report includes plots of time series, histograms, FFT and autocorrelations for the three coordinate components latitude, longitude and height. The stations are reported in alphabetical order. For most stations the results demonstrate a strong annual signature. This is however not unusual but found in most station time series from any continuously operational GNSS station anywhere on Earth. Obviously, the reason for these periodic variations should be found either in the data, the monumentation or possibly unmodeled parameters in the GNSS software. More than 30 years of continuous operation and data processing of a huge number of stations around the world has shown that periodic signature is visible in all times series. The most common is the yearly variations, basically visible in all timeseries but with a slight latitude dependence correlated with the GNSS satellite availability and geometry. It indicates that the root of the problem could be found in an error source common to all station i.e., the precise satellite orbits and clocks delivered by IGS, the underlying geophysical models or the definition of the reference frame (coordinate system). Annual signatures could also be due to snow and ice accumulation on top of the GNSS antennas, especially in high-latitude regions. Snow accumulation on top of the GNSS antenna could, in the GNSS software, be perceived as a signal propagation delay caused by the atmosphere leading to erroneous results. The snow accumulation can be serious problem during winter time at high-latitude stations. For inland stations in northern part of SWEPOS, this is probably the most significant contribution to the strong annual signal found especially in the height component of the coordinate results. The processing method PPP used in the GipsyX software package has no possibility to detect and mitigate snow accumulation. Instead, it will be absorbed by the parameters that GipsyX actually have been programmed to estimate. This means that parameters like the height component, together with ZTD, will absorb the “snow effect” and consequently provide erroneous estimates of these parameters.

Other rather common frequencies visible in the FFT plots (e.g., 14- or 28-days periodicities) are most likely connected to tidal effect (Earth Tides and Ocean Tidal Loading). This indicates that there are still possibilities to improve the geophysical models used by GNSS software packages such GipsyX and the Bernese software. Due to the long de-correlation time of GNSS data, the uncertainties given by the software is too optimistic. Instead, the day-to-day repeatability of the results is a more appropriate and realistic way of expressing the uncertainties of the results. From the timeseries and the histograms we can conclude that this “true” uncertainty, repeatability, in PPP processing of GNSS data is around 2 and 6 millimeters for the horizontal and vertical coordinate components, respectively. The main limiting factors are IGS satellites orbits and clocks, local effects such as multipath, snow and possible unstable monumentation and monument wander. Monument wander is the local motion of the ground to which the monument is attached. This is, most likely, not a problem in Sweden where we have the monuments attached to bed rock.

All the plots in the following subsections are supposed to give answers to important questions.

1. Do all the results have a normal distribution? The answer YES is given by the histograms.
2. Is the measurement noise generally “white”? The FFT plots show that the answer is NO and that the dominating noise is the annual periodic signature found at Index 3 on the X axis i.e., something that happens 3 times per 3 years (once per year).
3. Are the daily results “independent” or do we have day-to-day correlation? The answer is NO. All autocorrelation plots show strong correlation over ± 2–3 days, sometimes more.

3.2.1 Kobben (KOB0)

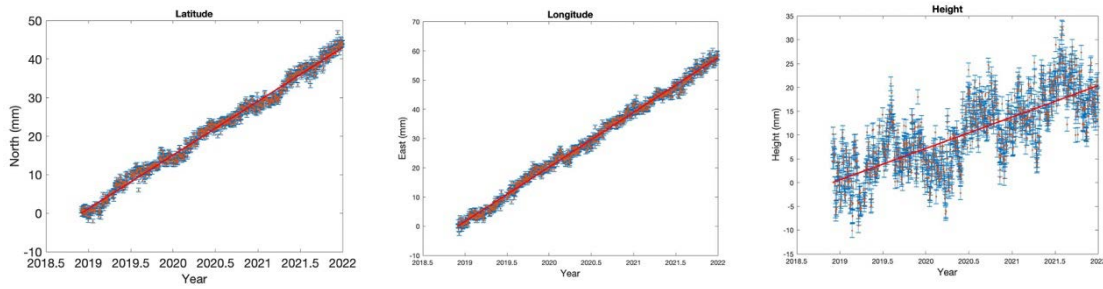


Figure 3-4. Daily KOB0 coordinate solutions with RMS error bars (left to right: Latitude, Longitude and Height) 2019–2021. In red, a model of the station motion using linear regression, is indicated. See Table 3-1 for the estimated station velocities and their respective uncertainty.

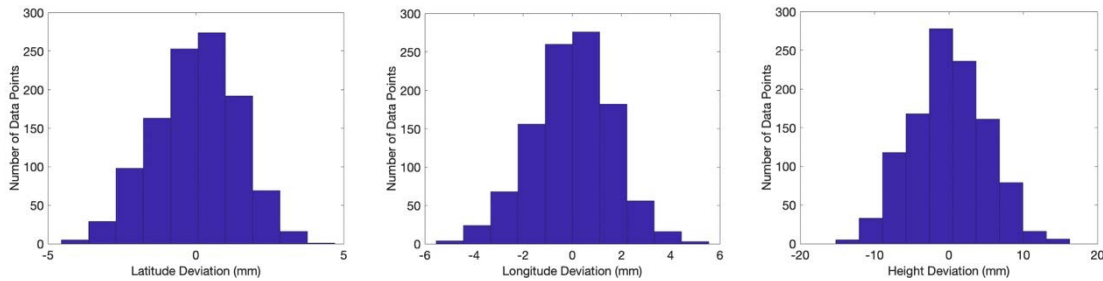


Figure 3-5. Difference between the daily results and the model represented as the red line in Figure 3-4. From left to right Latitude, Longitude and Height.

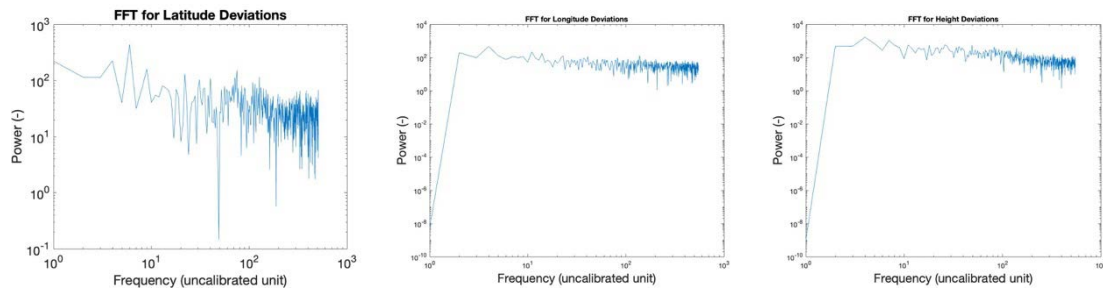


Figure 3-6. FFT of the difference between the daily results and the model represented as the red line in Figure 3-4. From left to right Latitude, Longitude and Height. Annual signatures are visible at Index 3 on the X axis since the periodicity is 3 peaks per three years.

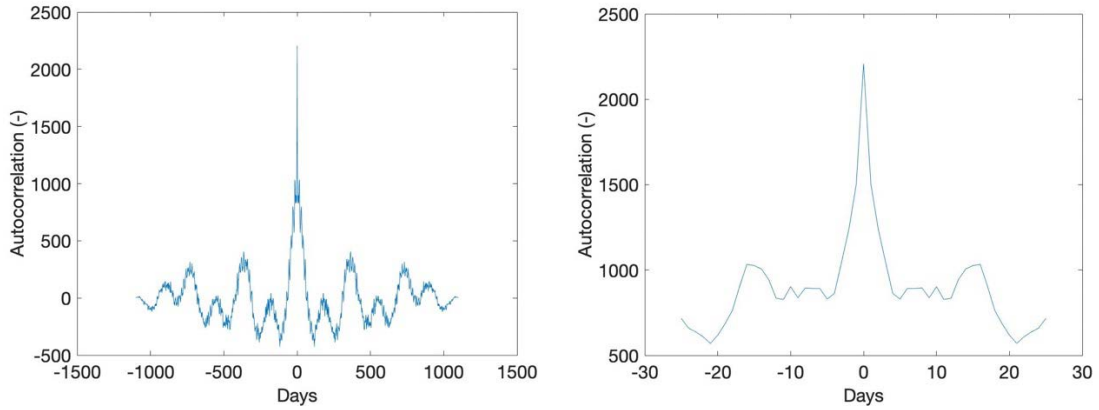


Figure 3-7. Autocorrelation of the Latitude difference between the daily results and the model represented as the red line in Figure 3-4. Full range is shown to the left and zooming in on ± 30 days in order to find the decorrelation time (Width in days at half power of the middle peak).

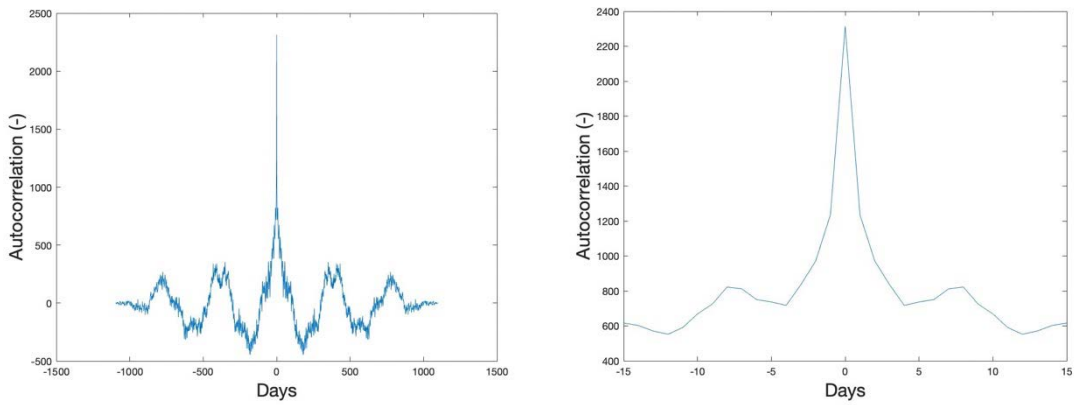


Figure 3-8. Autocorrelation of the Longitude difference between the daily results and the model represented as the red line in Figure 3-4. Full range is shown to the left and zooming in on ± 15 days in order to find the decorrelation time (Width in days at half power of the middle peak).

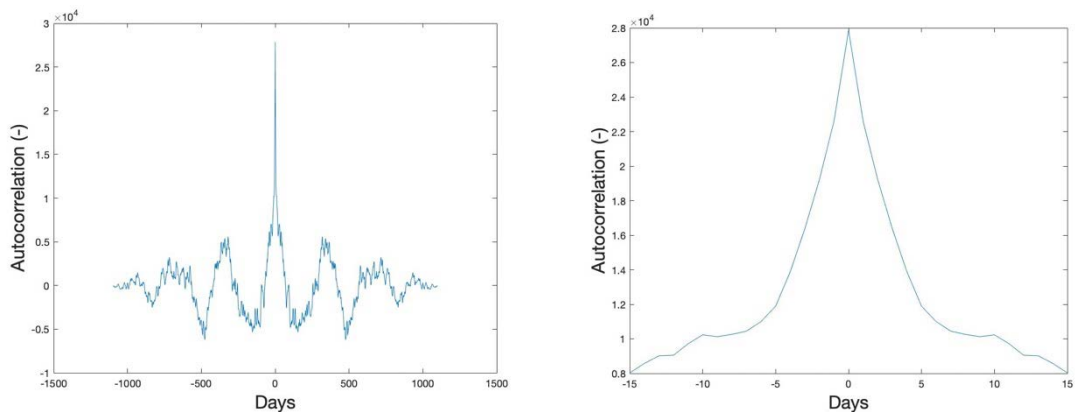


Figure 3-9. Autocorrelation of the Height difference between the daily results and the model represented as the red line in Figure 3-4. Full range is shown to the left and zooming in on ± 15 days in order to find the decorrelation time (Width in days at half power of the middle peak).

3.2.2 Lillkoben (LKB0)

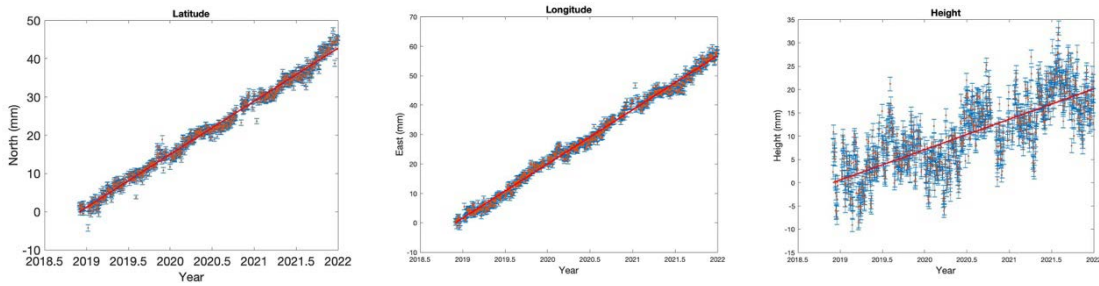


Figure 3-10. Daily LKB0 coordinate solutions with RMS error bars (left to right: Latitude, Longitude and Height) 2019–2021. In red, a model of the station motion using linear regression, is indicated. See Table 3-1 for the estimated station velocities and their respective uncertainty.

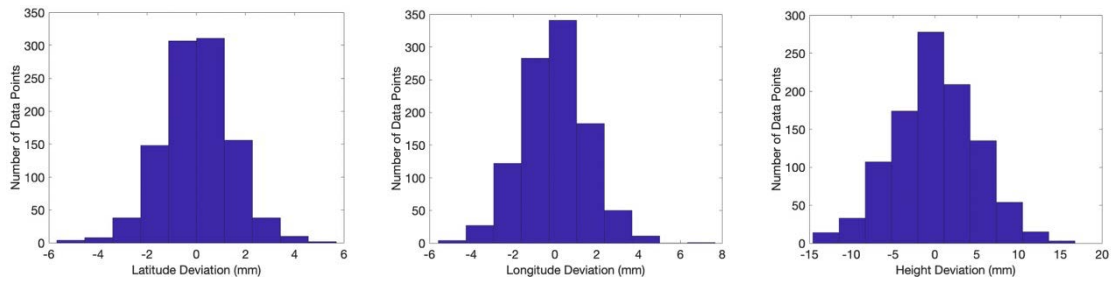


Figure 3-11. Difference between the daily results and the model represented as the red line in Figure 3-10. From left to right Latitude, Longitude and Height.

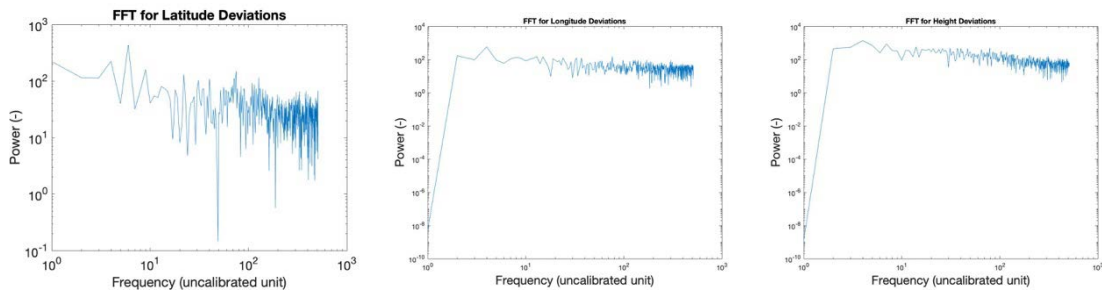


Figure 3-12. FFT of the difference between the daily results and the model represented as the red line in Figure 3-10. From left to right Latitude, Longitude and Height. Annual signatures are visible at Index 3 on the X axis since the periodicity is 3 peaks per three years.

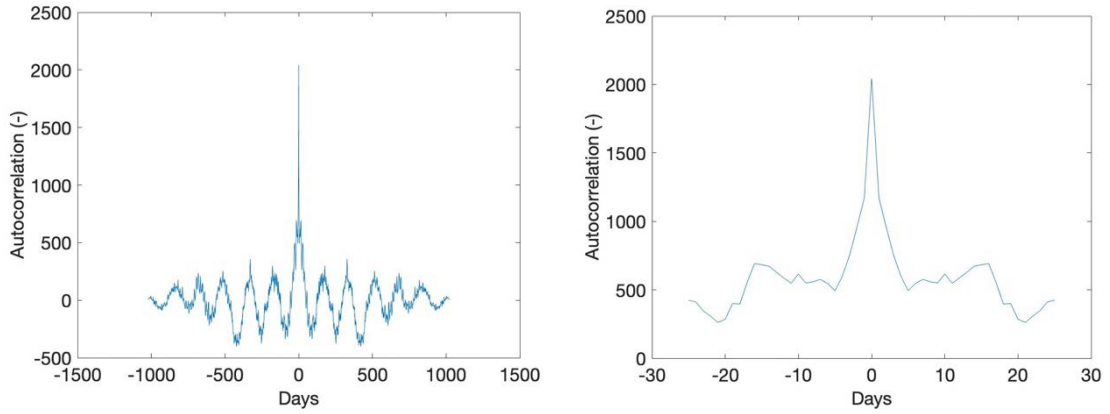


Figure 3-13. Autocorrelation of the Latitude difference between the daily results and the model represented as the red line in Figure 3-10. Full range is shown to the left and zooming in on ± 30 days in order to find the decorrelation time (Width in days at half power of the middle peak).

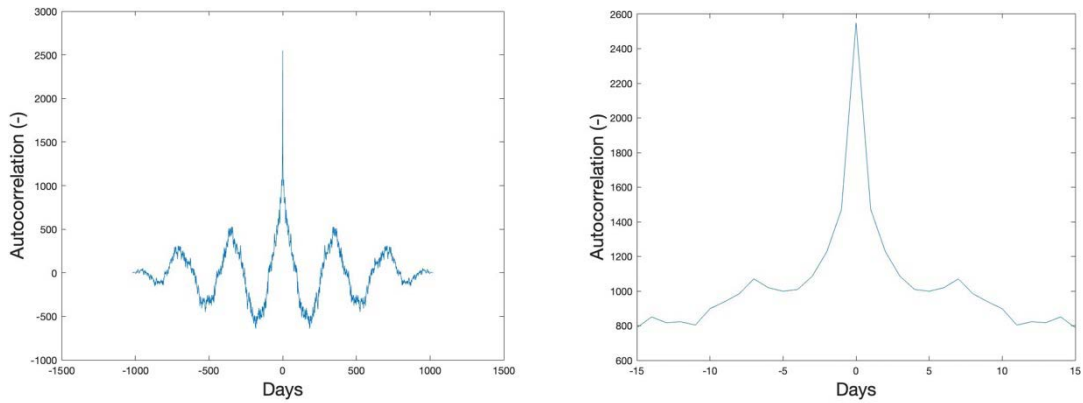


Figure 3-14. Autocorrelation of the Longitude difference between the daily results and the model represented as the red line in Figure 3-10. Full range is shown to the left and zooming in on ± 15 days in order to find the decorrelation time (Width in days at half power of the middle peak).

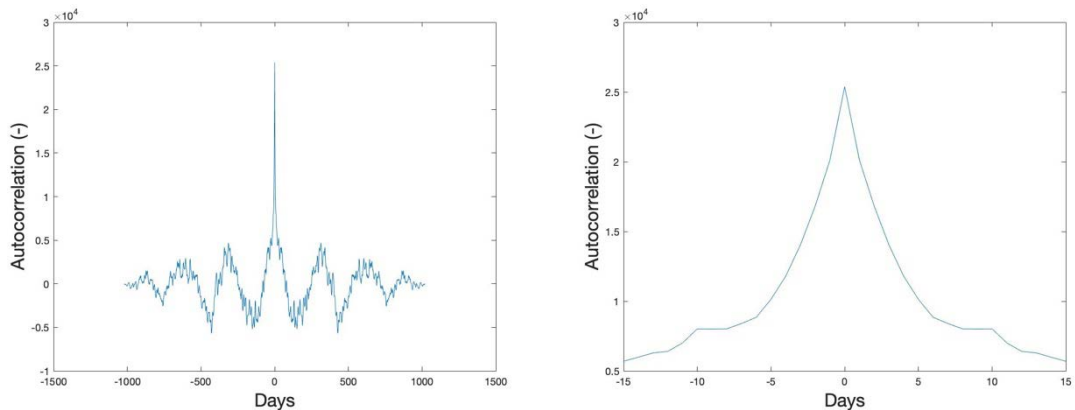


Figure 3-15. Autocorrelation of the Height difference between the daily results and the model represented as the red line in Figure 3-10. Full range is shown to the left and zooming in on ± 15 days in order to find the decorrelation time (Width in days at half power of the middle peak).

3.2.3 Norra Biotesten (NB10)

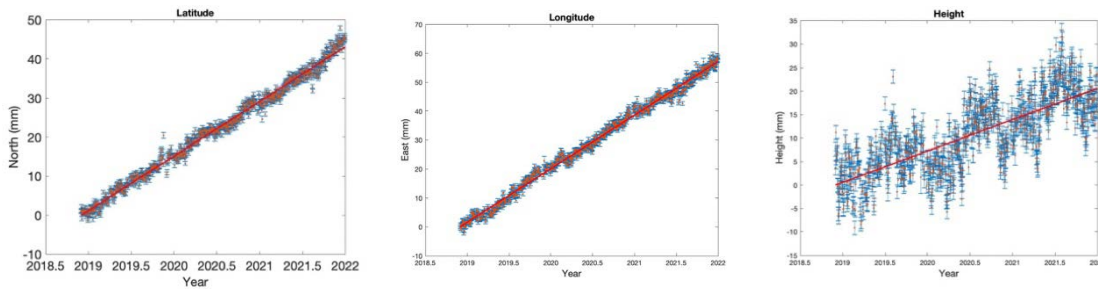


Figure 3-16. Daily NB10 coordinate solutions with RMS error bars (left to right: Latitude, Longitude and Height) 2019–2021. In red, a model of the station motion using linear regression, is indicated. See Table 3-1 for the estimated station velocities and their respective uncertainty.

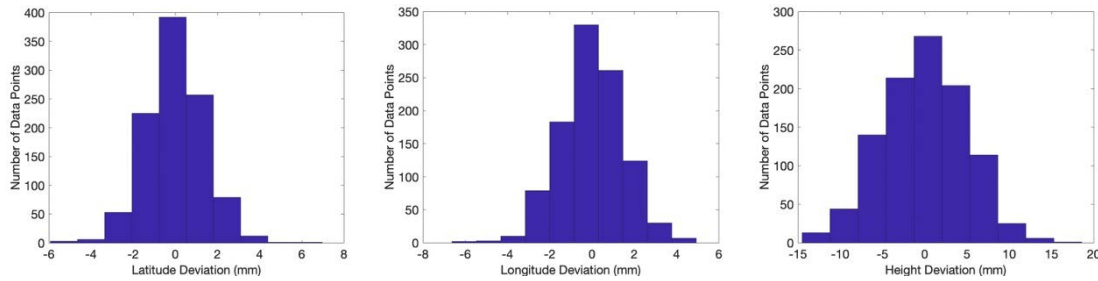


Figure 3-17. Difference between the daily results and the model represented as the red line in Figure 3-16. From left to right Latitude, Longitude and Height.

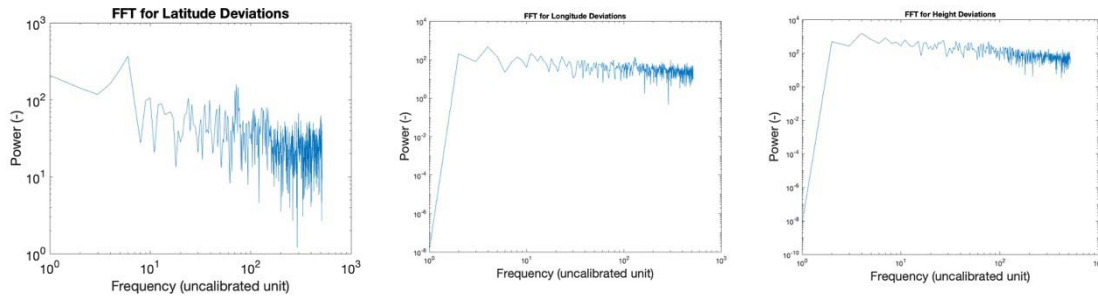


Figure 3-18. FFT of the difference between the daily results and the model represented as the red line in Figure 3-16. From left to right Latitude, Longitude and Height. Annual signatures are visible at Index 3 on the X axis since the periodicity is 3 peaks per three years.

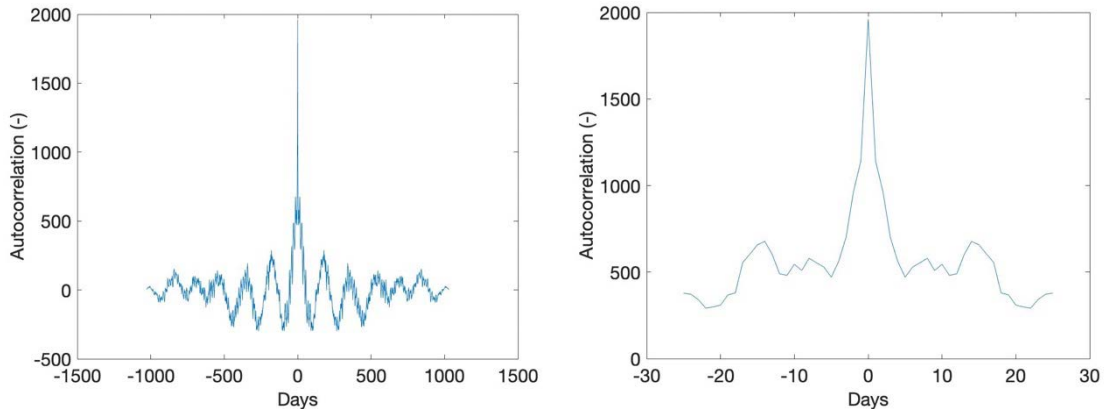


Figure 3-19. Autocorrelation of the Latitude difference between the daily results and the model represented as the red line in Figure 3-16. Full range is shown to the left and zooming in on ± 30 days in order to find the decorrelation time (Width in days at half power of the middle peak).

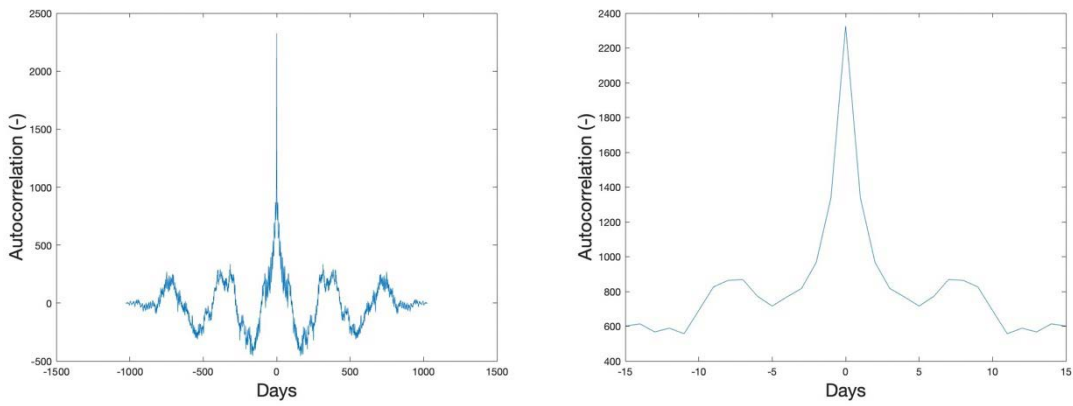


Figure 3-20. Autocorrelation of the Longitude difference between the daily results and the model represented as the red line in Figure 3-16. Full range is shown to the left and zooming in on ± 15 days in order to find the decorrelation time (Width in days at half power of the middle peak).

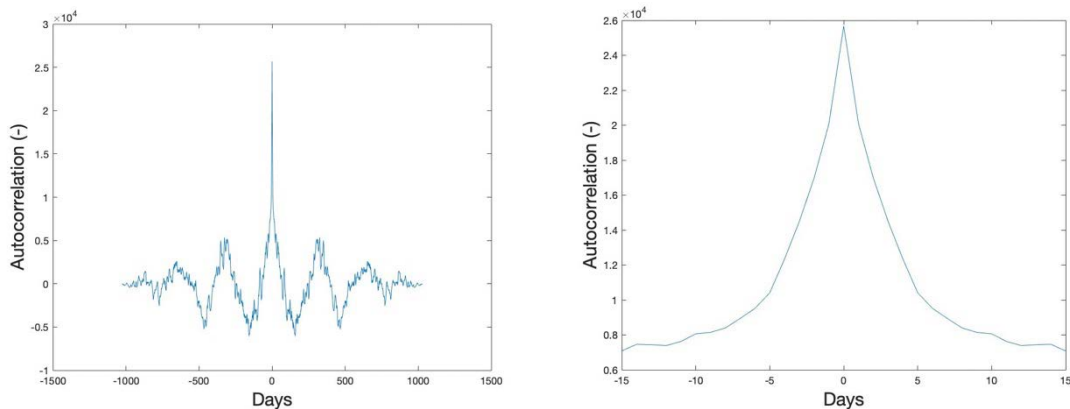


Figure 3-21. Autocorrelation of the Height difference between the daily results and the model represented as the red line in Figure 3-16. Full range is shown to the left and zooming in on ± 15 days in order to find the decorrelation time (Width in days at half power of the middle peak).

3.2.4 Söderboda (SOD0)

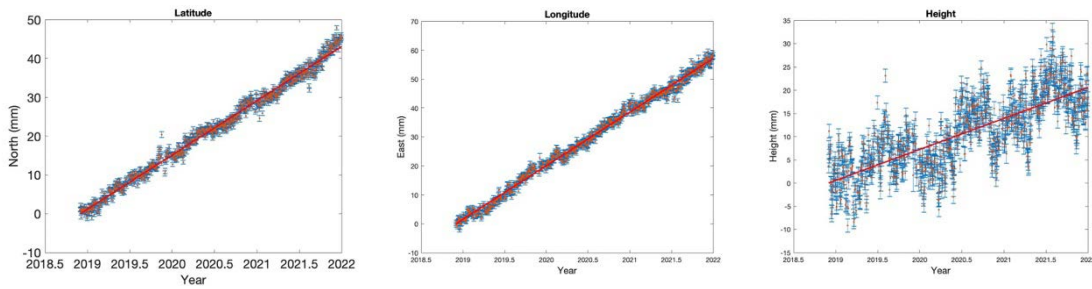


Figure 3-22. Daily SOD0 coordinate solutions with RMS error bars (left to right: Latitude, Longitude and Height) 2019–2021. In red, a model of the station motion using linear regression, is indicated. See Table 3-1 for the estimated station velocities and their respective uncertainty. Note that this is a SWEPOS station not included in the SKB network but used as reference. The station is equipped with the SWEPOS standard steel grid mast.

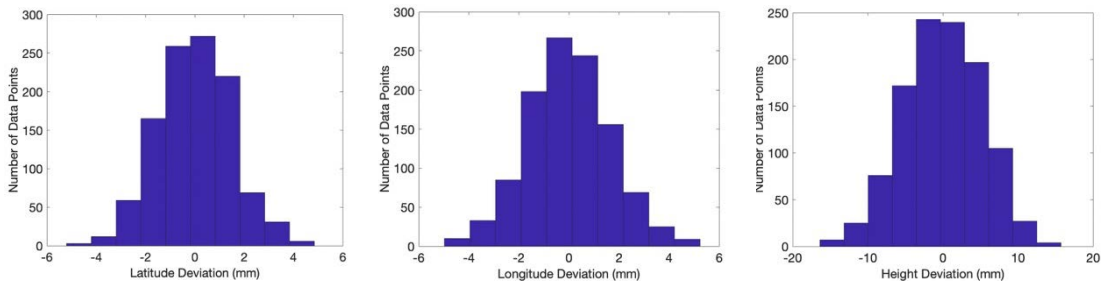


Figure 3-23. Difference between the daily results and the model represented as the red line in Figure 3-22. From left to right Latitude, Longitude and Height.

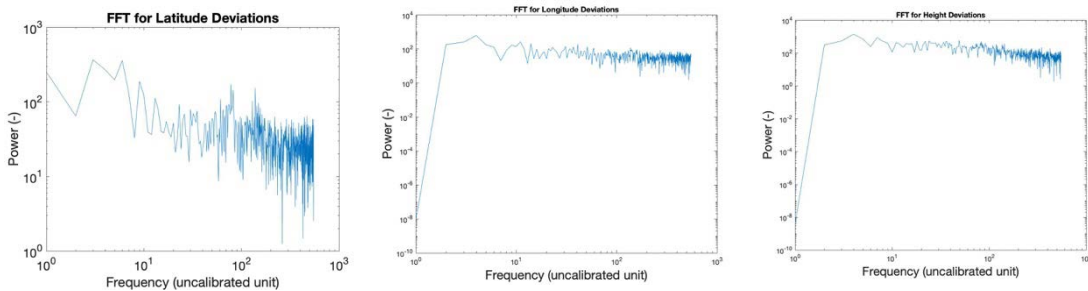


Figure 3-24. FFT of the difference between the daily results and the model represented as the red line in Figure 3-22. From left to right Latitude, Longitude and Height. Annual signatures are visible at Index 3 on the X axis since the periodicity is 3 peaks per three years.

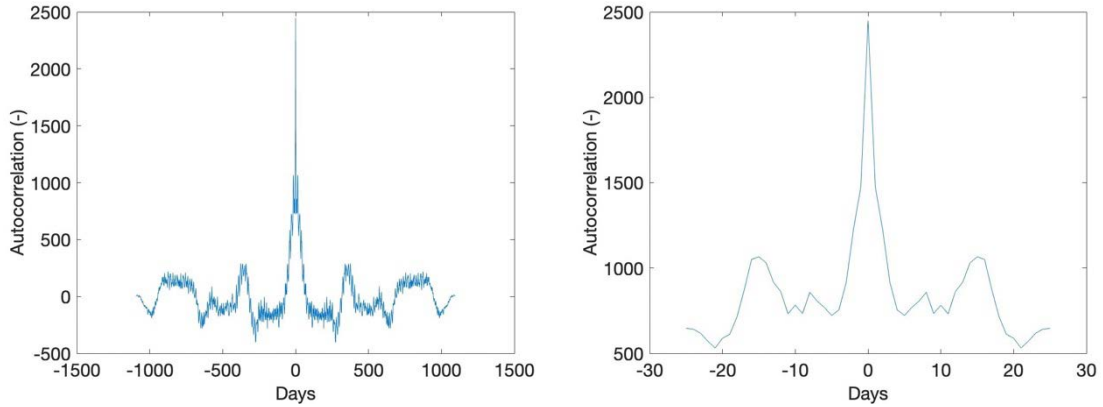


Figure 3-25. Autocorrelation of the Latitude difference between the daily results and the model represented as the red line in Figure 3-22. Full range is shown to the left and zooming in on ± 30 days in order to find the decorrelation time (Width in days at half power of the middle peak).

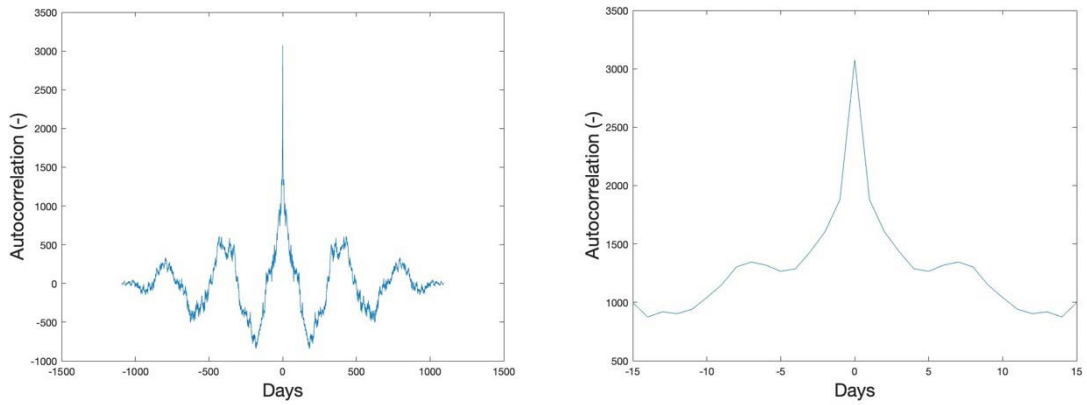


Figure 3-26. Autocorrelation of the Longitude difference between the daily results and the model represented as the red line in Figure 3-22. Full range is shown to the left and zooming in on ± 15 days in order to find the decorrelation time (Width in days at half power of the middle peak).

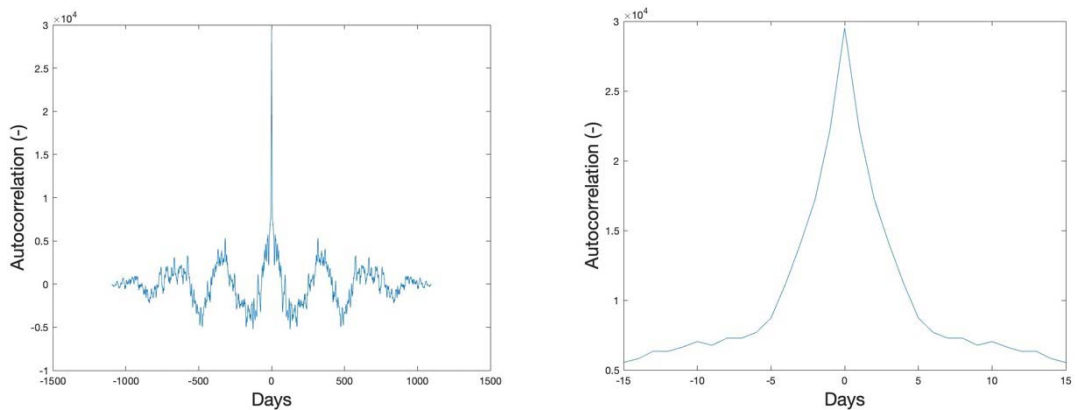


Figure 3-27. Autocorrelation of the Height difference between the daily results and the model represented as the red line in Figure 3-22. Full range is shown to the left and zooming in on ± 15 days in order to find the decorrelation time (Width in days at half power of the middle peak).

3.2.5 Storskäret (SSK0)

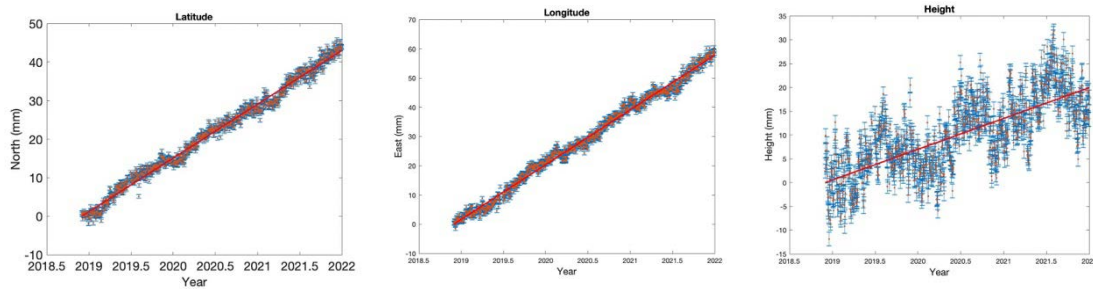


Figure 3-28. Daily SSK0 coordinate solutions with RMS error bars (left to right: Latitude, Longitude and Height) 2019–2021. In red, a model of the station motion using linear regression, is indicated. See Table 3-1 for the estimated station velocities and their respective uncertainty.

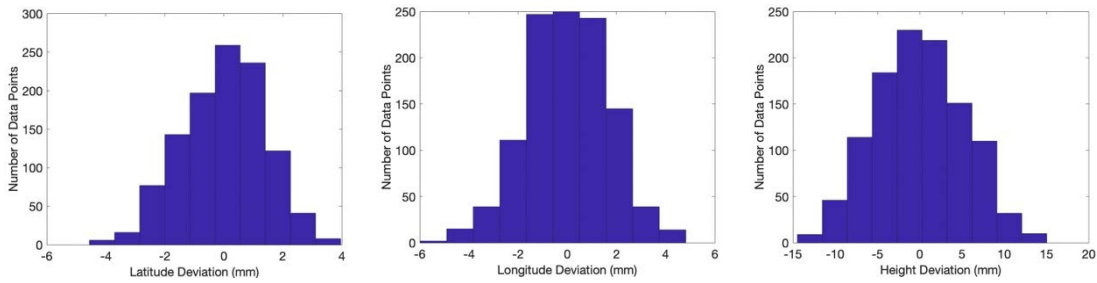


Figure 3-29. Difference between the daily results and the model represented as the red line in Figure 3-28. From left to right Latitude, Longitude and Height.

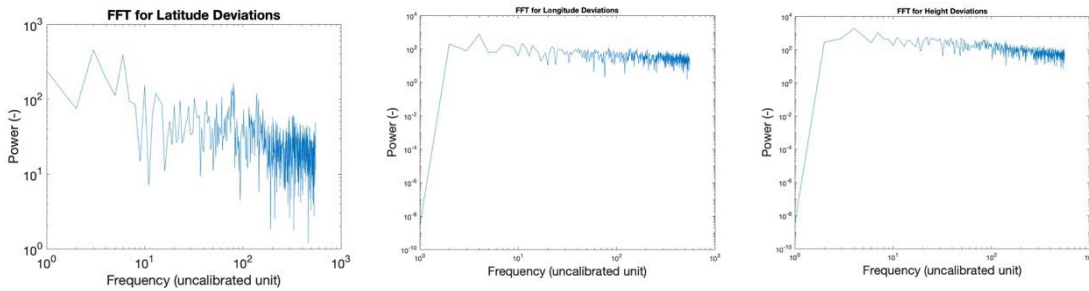


Figure 3-30. FFT of the difference between the daily results and the model represented as the red line in Figure 3-28. From left to right Latitude, Longitude and Height. Annual signatures are visible at Index 3 on the X axis since the periodicity is 3 peaks per three years.

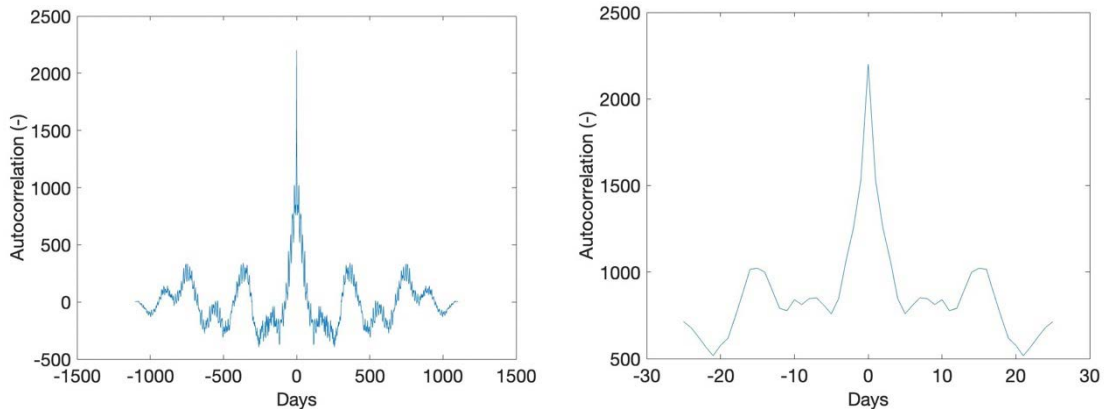


Figure 3-31. Autocorrelation of the Latitude difference between the daily results and the model represented as the red line in Figure 3-28. Full range is shown to the left and zooming in on ± 30 days in order to find the decorrelation time (Width in days at half power of the middle peak).

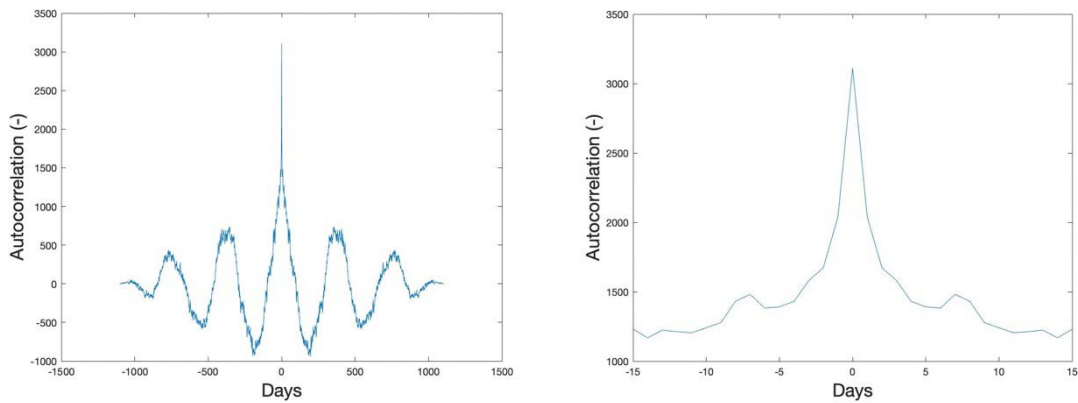


Figure 3-32. Autocorrelation of the Longitude difference between the daily results and the model represented as the red line in Figure 3-28. Full range is shown to the left and zooming in on ± 15 days in order to find the decorrelation time (Width in days at half power of the middle peak).

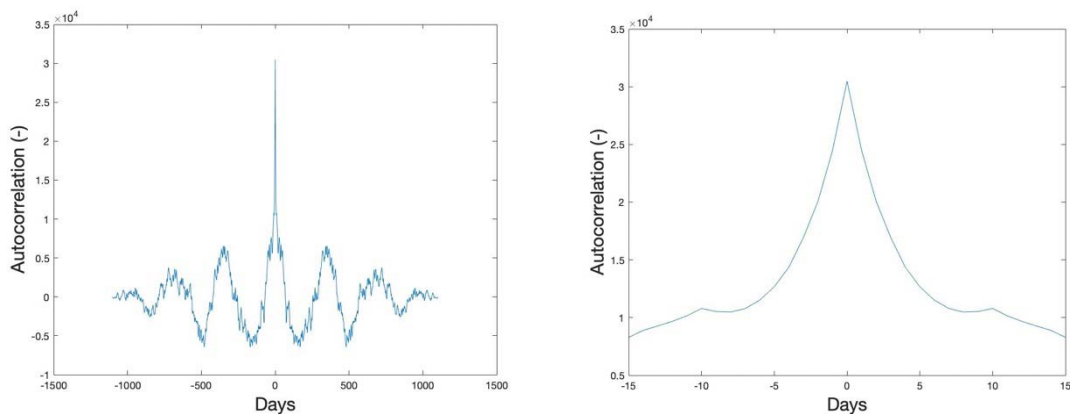


Figure 3-33. Autocorrelation of the Height difference between the daily results and the model represented as the red line in Figure 3-28. Full range is shown to the left and zooming in on ± 15 days in order to find the decorrelation time (Width in days at half power of the middle peak).

3.2.6 Uppsala (UPP0)

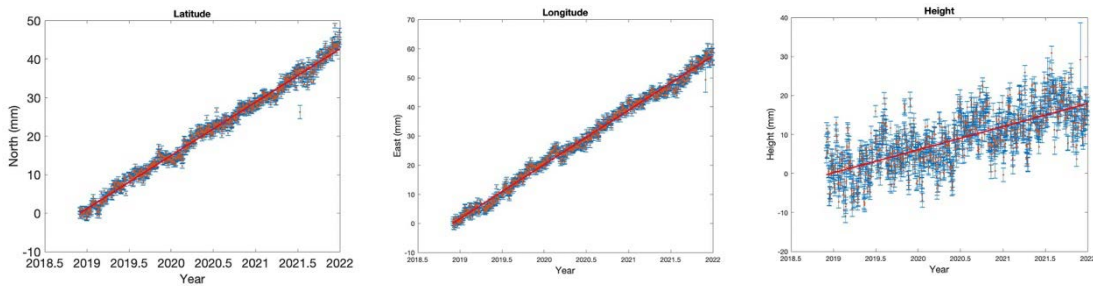


Figure 3-34. Daily UPP0 coordinate solutions with RMS error bars (left to right: Latitude, Longitude and Height) 2019–2021. In red, a model of the station motion using linear regression, is indicated. See Table 3-1 for the estimated station velocities and their respective uncertainty. Note that this is a SWEPOS station not included in the SKB network but used as reference. The station is equipped with the SWEPOS standard concrete pillar monument.

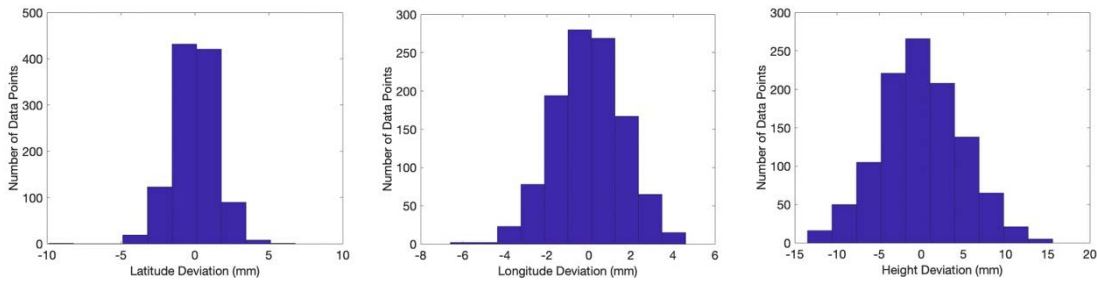


Figure 3-35. Difference between the daily results and the model represented as the red line in Figure 3-34. From left to right Latitude, Longitude and Height.

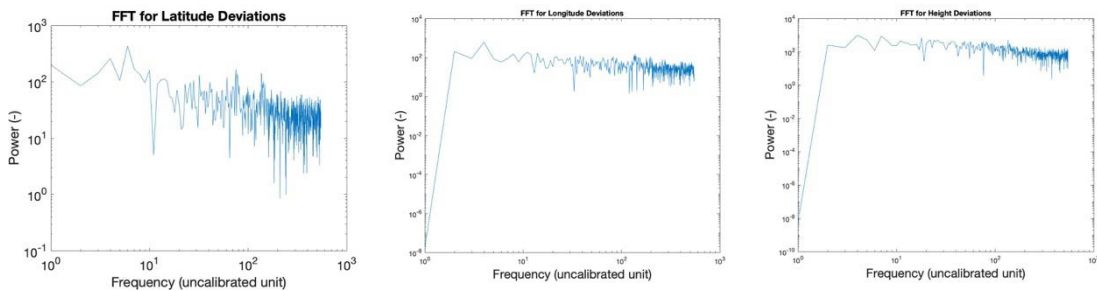


Figure 3-36. FFT of the difference between the daily results and the model represented as the red line in Figure 3-34. From left to right Latitude, Longitude and Height. Annual signatures are visible at Index 3 on the X axis since the periodicity is 3 peaks per three years.

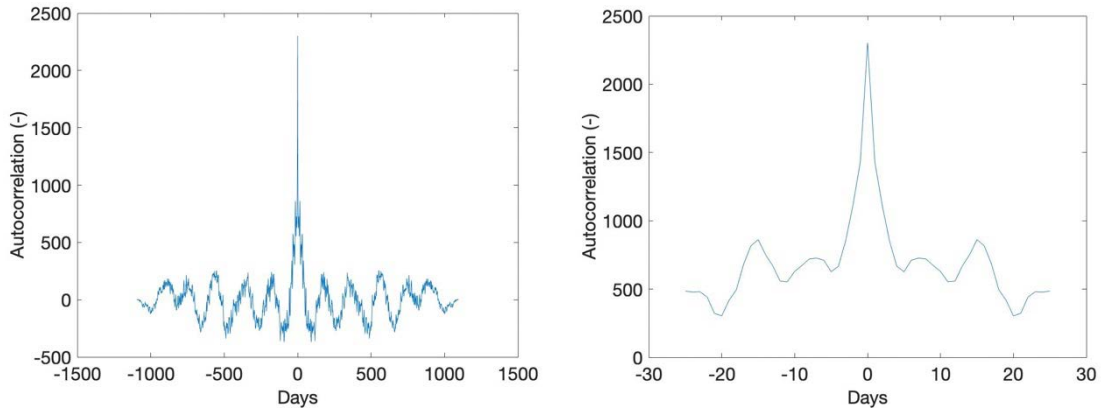


Figure 3-37. Autocorrelation of the Latitude difference between the daily results and the model represented as the red line in Figure 3-34. Full range is shown to the left and zooming in on ± 30 days in order to find the decorrelation time (Width in days at half power of the middle peak).

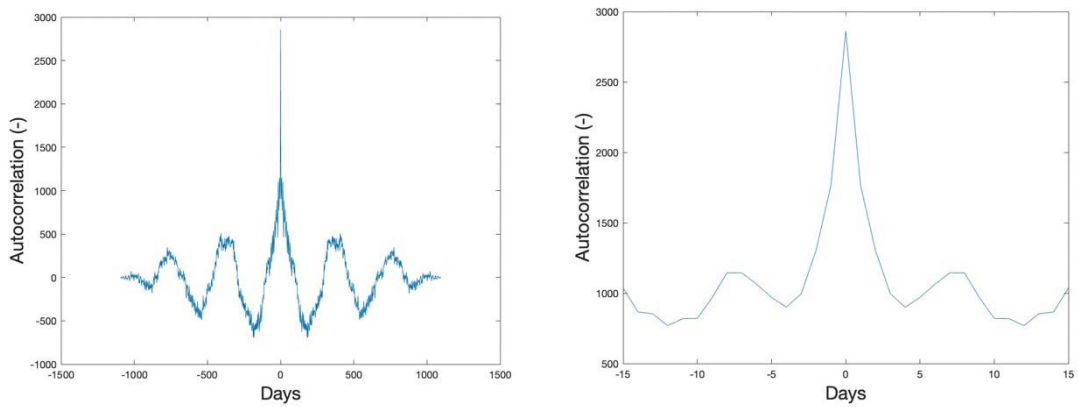


Figure 3-38. Autocorrelation of the Longitude difference between the daily results and the model represented as the red line in Figure 3-34. Full range is shown to the left and zooming in on ± 15 days in order to find the decorrelation time (Width in days at half power of the middle peak).

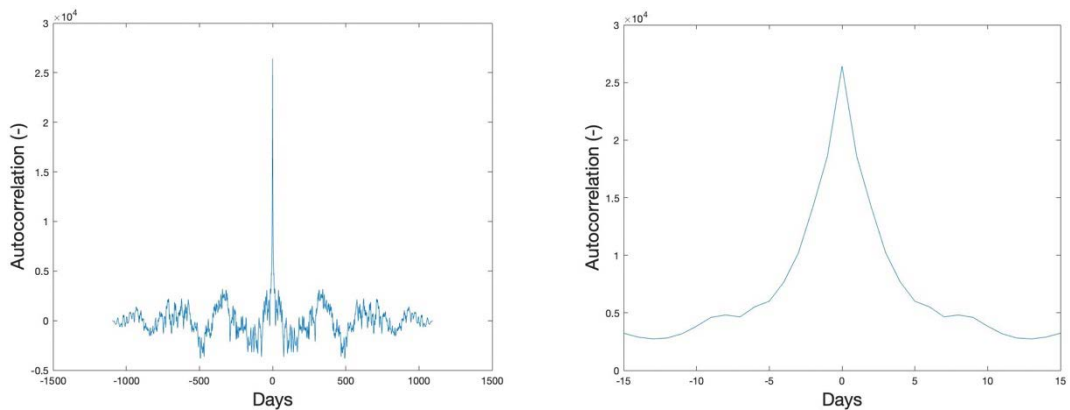


Figure 3-39. Autocorrelation of the Height difference between the daily results and the model represented as the red line in Figure 3-34. Full range is shown to the left and zooming in on ± 15 days in order to find the decorrelation time (Width in days at half power of the middle peak).

3.2.7 Västra Måsklinten (VMA0)

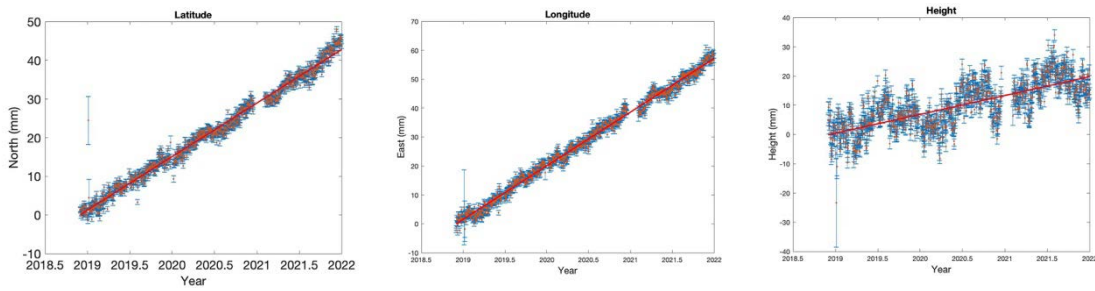


Figure 3-40. Daily UPP0 coordinate solutions with RMS error bars (left to right: Latitude, Longitude and Height) 2019–2021. In red, a model of the station motion using linear regression, is indicated. See Table 3-1 for the estimated station velocities and their respective uncertainty.

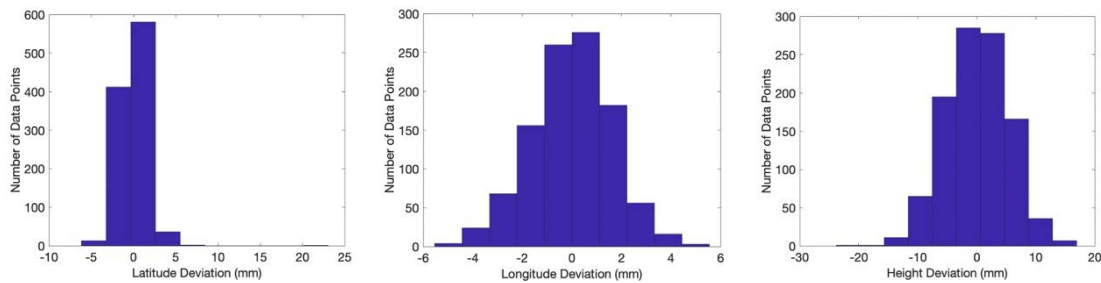


Figure 3-41. Difference between the daily results and the model represented as the red line in Figure 3-40. From left to right Latitude, Longitude and Height.

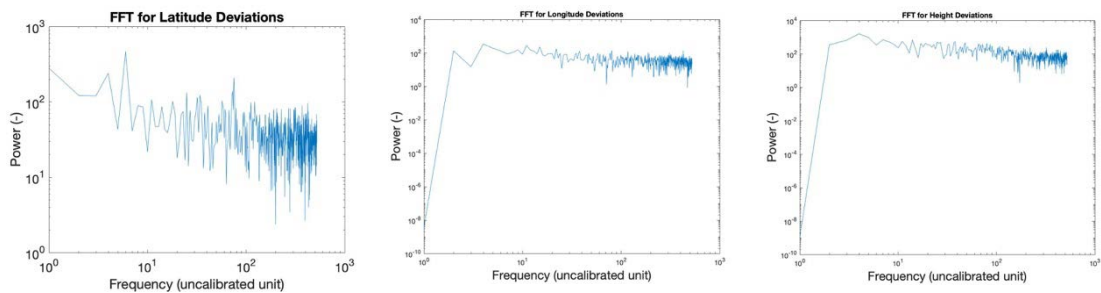


Figure 3-42. FFT of the difference between the daily results and the model represented as the red line in Figure 3-40. From left to right Latitude, Longitude and Height. Annual signatures are visible at Index 3 on the X axis since the periodicity is 3 peaks per three years.

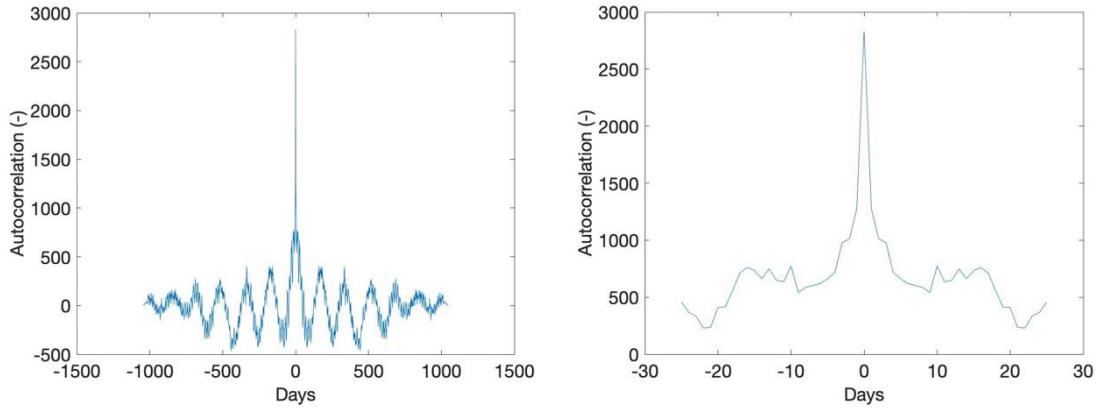


Figure 3-43. Autocorrelation of the Latitude difference between the daily results and the model represented as the red line in Figure 3-40. Full range is shown to the left and zooming in on ± 30 days in order to find the decorrelation time (Width in days at half power of the middle peak).

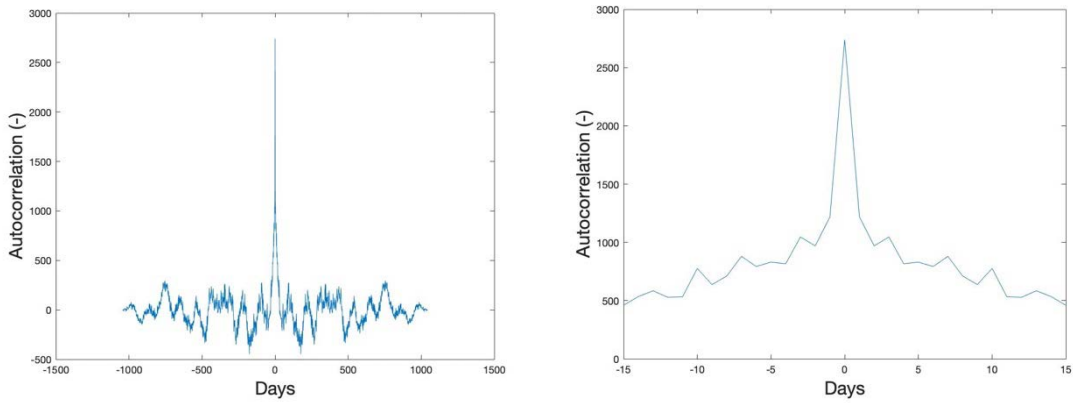


Figure 3-44. Autocorrelation of the Longitude difference between the daily results and the model represented as the red line in Figure 3-40. Full range is shown to the left and zooming in on ± 15 days in order to find the decorrelation time (Width in days at half power of the middle peak).

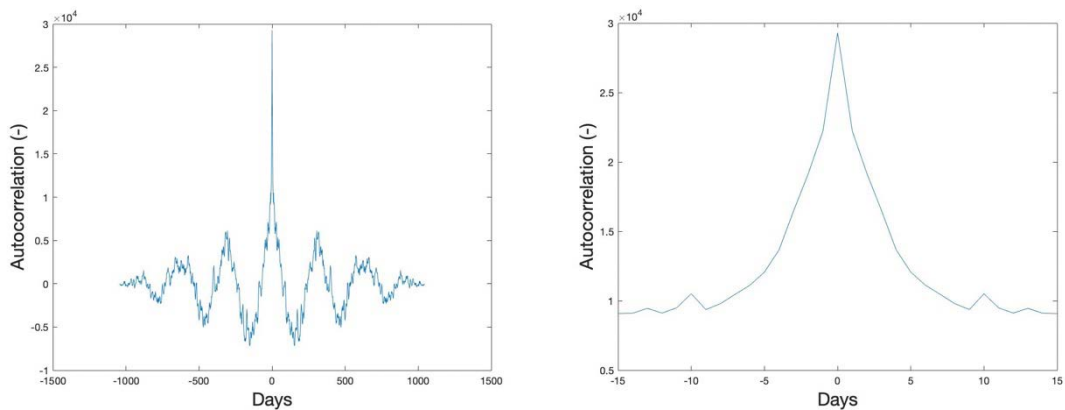


Figure 3-45. Autocorrelation of the Height difference between the daily results and the model represented as the red line in Figure 3-40. Full range is shown to the left and zooming in on ± 15 days in order to find the decorrelation time (Width in days at half power of the middle peak).

3.3 Baseline investigation

All reported results in Section 3.2 are based on PPP analysis of GNSS data from GPS, Glonass and Galileo. As the PPP method is used the data analysis is only performed for one station at a time and there is no connection at the observational level between stations. However, this “connection” is usually present in most other GNSS software, such as the Bern software, where data from all stations in the network are included in the same analysis and where so-called single and double differences between station and satellite pairs are formed. Single and double differences are formed at the observation level, which directly result in three-dimensional distances between the stations.

Such station distances do not come directly from the PPP data analysis because only one station is analyzed at a time. In order to look at three-dimensional distances between stations in a GNSS network, one must analyze all the stations separately and then calculate the station distances. This is, however, not a mathematically optimal way to go because you use the coordinate results for each station to calculate three-dimensional distances for each day. Although each station’s daily coordinate estimate mainly suffers from common sources of error such as satellite orbits and satellite clocks, some days may also be affected by local errors. If the errors are common, they will be largely eliminated when looking at the distance between station pairs while local errors do not get the same favor.

A common local error that affects the coordinate results is snow accumulation on the GNSS antenna during the winter. To some extent, condensation and icing on the radome that protects the GNSS antenna can also lead to systematic errors over shorter or longer periods of time.

One type of error that has been under discussion for more than thirty years are those related to the stability of GNSS monuments. Several scientific papers have been published in which a large number of GNSS monuments have been evaluated using various methods. Also, for SWEPOS, in connection with the land uplift project BIFROST (Johansson et al. 2002, Lidberg et al. 2007, Kierulf et al. 2021), the stations’ various antenna monuments (foundations) have been evaluated. In most of these investigations the data quality and the uncertainty of the final coordinate estimates have been too high in order to investigate possible small (± 1 millimeter) monument motion using only the GNSS data themselves. Monitoring of “monument wander” could also be carried out using other techniques e.g., laser instruments and such investigations are ongoing at RISE and AstaZero (<https://www.astazero.com/>) as well as at Chalmers with Onsala Space Observatory (<https://www.chalmers.se/sv/institutioner/see/forskning/oso/>).

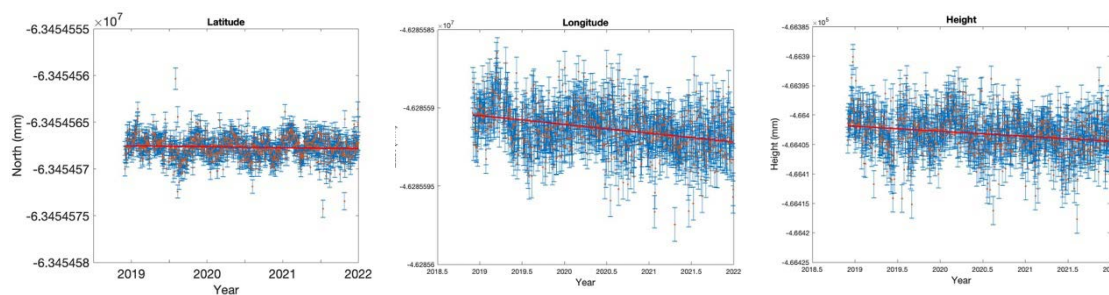


Figure 3-46. Estimated three-dimensional baseline between the SWEPOS station SOD0 (steel grid mast) and UPP0 (concrete pillar) with RMS error bars (left to right: Latitude, Longitude and Height) 2019–2021. In red, the estimated station motion is indicated (available on request).

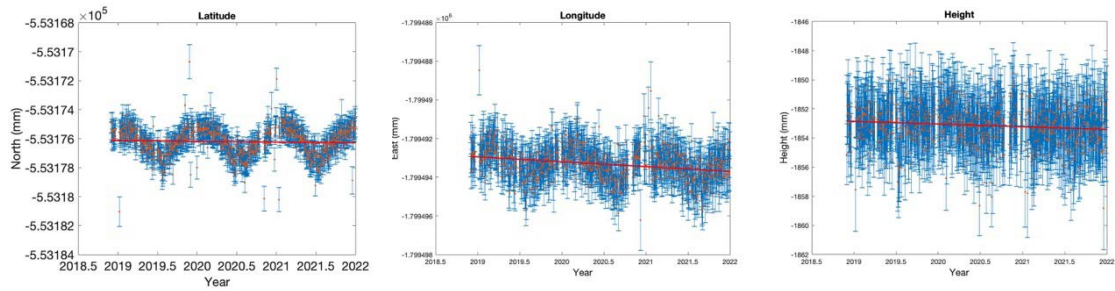


Figure 3-47. Estimated three-dimensional baseline between the SKB stations KOB0 and LKB0 (both equipped with steel grid mast) with RMS error bars (left to right: Latitude, Longitude and Height) 2019–2021. In red, the estimated station motion is indicated (available on request).

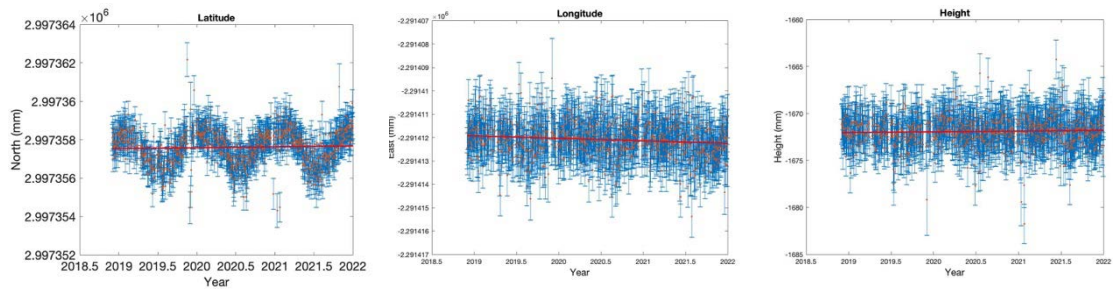


Figure 3-48. Estimated three-dimensional baseline between the SKB stations KOB0 and NBI0 (both equipped with steel grid mast) with RMS error bars (left to right: Latitude, Longitude and Height) 2019–2021. In red, the estimated station motion is indicated (available on request).

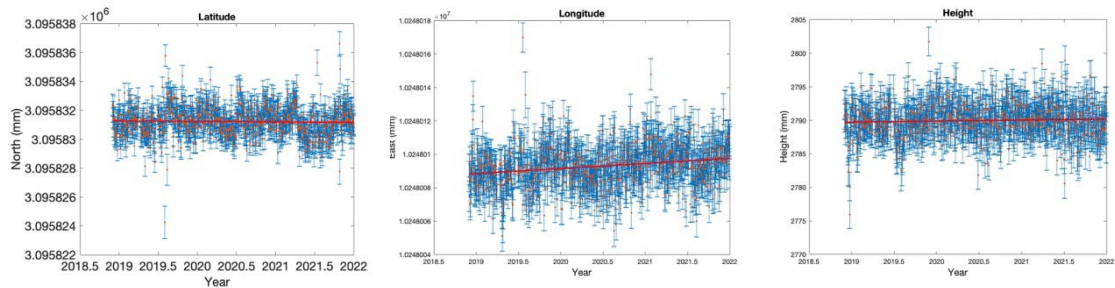


Figure 3-49. Estimated three-dimensional baseline between the SKB station KOB0 and the SWEPOS station SOD0 (both equipped with steel grid mast) with RMS error bars (left to right: Latitude, Longitude and Height) 2019–2021. In red, the estimated station motion is indicated (available on request).

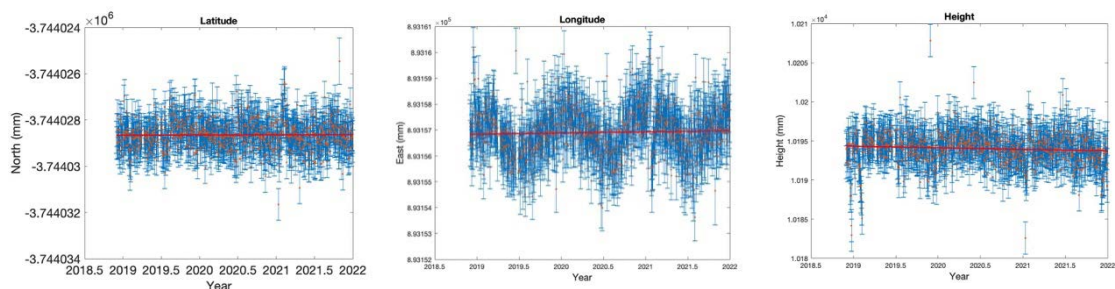


Figure 3-50. Estimated three-dimensional baseline between the SKB stations KOB0 and SSK0 (both equipped with steel grid masts but of different kind) with RMS error bars (left to right: Latitude, Longitude and Height) 2019–2021. In red, the estimated station motion is indicated (available on request).

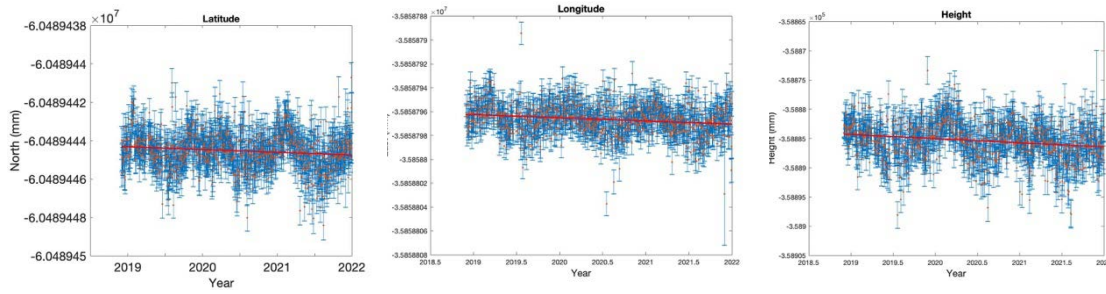


Figure 3-51. Estimated three-dimensional baseline between the SKB stations KOB0 (equipped with standard steel grid mast) and UPP0 (concrete pillar) with RMS error bars (left to right: Latitude, Longitude and Height) 2019–2021. In red, the estimated station motion is indicated (available on request).

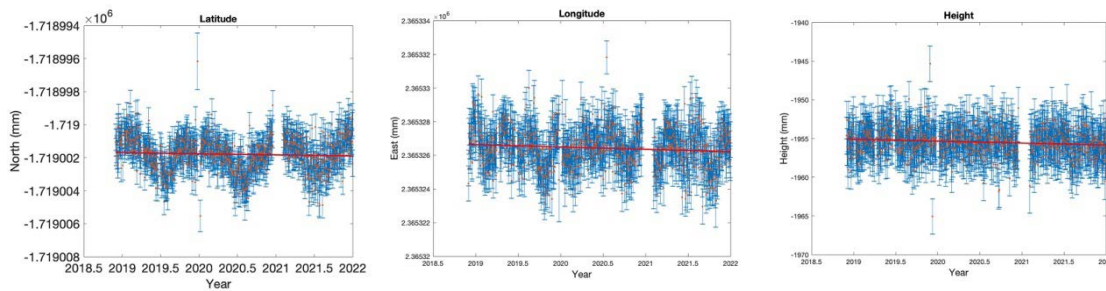


Figure 3-52. Estimated three-dimensional baseline between the SKB stations KOB0 and VMA0 (both equipped with steel grid masts but of different kind) with RMS error bars (left to right: Latitude, Longitude and Height) 2019–2021. In red, the estimated station motion is indicated (available on request).

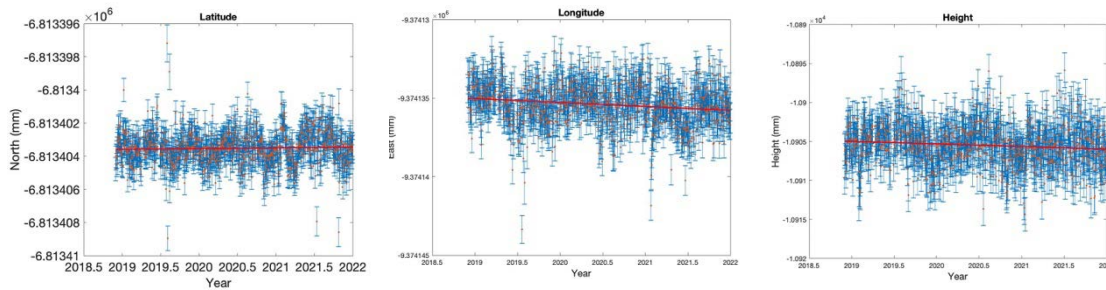


Figure 3-53. Estimated three-dimensional baseline between the SWEPOS station SOD0 (equipped with SWEPOS steel grid mast) and the SKB station SSK0 (equipped with special kind of steel grid mast) with RMS error bars (left to right: Latitude, Longitude and Height) 2019–2021. In red, the estimated station motion is indicated (available on request).

4 Discussion and Conclusions

The SKB network was setup in 2018 using state-of-the-art GNSS receiving systems and monumentation. This has resulted in a 5-station network delivering high-quality data from all GNSS. Due to the exceptionally high data quality and short interstation distances in the SKB network it offers a unique opportunity for deeper investigations of monument stability using the GNSS data and results themselves. Looking at the Figures 3-47, 3-48, 3-50 and 3-52, all showing three-dimensional baseline results between SKB stations indicate unsurpassed data quality giving possibilities to identify seasonal variations at the submillimeter level.

For comparison we also include Figure 3-46 showing a baseline between SWEPOS station in the region around Forsmark. The two stations Söderboda (SOD0) and Uppsala (UPP0) seem to be less affected by seasonal effects. However, the noise level of the Uppsala station, a concrete pillar with a residual pattern according to Figure 3-3, is higher and could possibly shadow such variations.

Figures 3-49 and 3-53 are interesting since both baselines include SOD0 and one station in the SKB network. In Figure 3-49 the SKB station is KOB0, a standard SWEPOS pillar just like SOD0, and the results demonstrate a very clear annual signature. In Figure 3-53 the station pair is instead SOD0 together with SSK0 a SKB station but with a unique steel grid mast. Although different periodic signature may be identified in Figure 3-53, the seasonal variations do not have a strong amplitude.

However, the interpretation of baseline results is difficult. Partly because we are extremely close to the noise level of GNSS carrier data and partly because we cannot, in a difference between two stations, determine which monument/antenna is moving. In fact, both the antennas (masts) could be in motion and furthermore they could both simultaneously move in the same direction. If so, a possible motion will not be visible in the resulting plots. The results also depend on very sophisticated data analysis with the utilizing the PPP method. The analysis requires that all parameters and input data are correctly modelled. There is still reason to suspect that the analysis of GNSS data, shown in Figure 2-1, at this accuracy level requires improved geophysical models and more accurate satellite orbits and satellite clocks. On short baselines also the handling of the tropospheric propagation path delay parameter may have an influence on the results since the atmosphere at both sites in a station pair are very much correlated.

For future work we envision several types of studies. With the high GNSS data quality found in all SKB stations it is possible to continue the investigating the possible cause of the seasonal variations. The possible cause could be related to both thermal expansion in parts of the truss mast (see Figure 4-1) as well as an antenna related effect Figure 4-2. In the study by Lehner (2011) it was noted that the variations could be made smaller by shielding of monument, e.g., with a plastic pipe surrounding the steel grid mast. The drawback, and without totally eliminating the temperature problem, being the possible introduction of a new multipath environment similar those found at the concrete pillar stations such as Uppsala (UPP0) in Figure 3-3.

However, we cannot yet exclude the possibility that the “problem” could be found in our PPP GNSS data processing engine. The GNSS software packages are continuously updated with new models and data processing strategies.

For the future, we suggest that the dense local GNSS networks, with state-of-the-art equipment, available in Forsmark, Onsala Space Observatory and AstaZero are used for further investigations. At RISE test track AstaZero there is also possibility to monitor antenna/mast motions using laser instruments. This would give new insight to possible problems associated with the top part of the antenna i.e., the section between the antenna and the truss mast.

When using truss masts, it could be important to protect the mast foot in order to prevent from thermal expansion in the attachment to the bedrock, for example by laying the monuments on flat slabs and possibly thermally insulating them with Styrofoam. Regarding tests related to the steel grid mast we suggest trying to protect the mast foot at one SKB station (or a station at AstaZero) with Styrofoam over the summer 2023.

When establishing new stations in the SKB network, it is important to obtain as good observational conditions as possible by keeping a free horizon angle around all stations. This is obviously already the case for the existing stations. Another monument that could be used is shown in Figure 1-2, where the station in Smögen has a low pyramid-shaped concrete monument.

Another part of the receiving system at each GNSS station is the cable between the antenna and the receiver. Coaxial antenna cables with type N or TNC connectors are often used in GNSS permanent stations, also in SWEPOS. These cables have a fairly large temperature dependence and the cable lengths are often substantial (> 10 meters). This will result in a change of the signal time delay in the cable depending on the temperature. This could be mitigated by having shorter, better or more protected or insulated cables. However, the variations of the signal time delay in the cable will be absorbed by the receiver clock parameter estimated for example in the GipsyX PPP data analysis.

There are a huge number of different GNSS antennas for high-precision applications on the market. The most popular uses a so-called choke-ring design seen in Figure 4-2. Many of them actually use the same antenna element manufactured by the US company Dorne-Margolin Inc. Although the antenna element, a crossed microstrip dipole, is of high-quality there might be some small issues with the actual attachment of the antenna element to the rest of the antenna called the ground plane. The ground plane is a metallic construction giving protection so that reflected signals cannot sneak in to the antenna element from beneath. How the antenna element is attached to the antenna ground plane is the manufacturers secret and has not yet been thoroughly investigated. At the level of high-quality results achieved with the SKB network this, together with the monumentation, is something that needs further attentions

5. UNDERGJUTNING AV FOTPLATTOR

Undergjutning är ett garantivillkor. Efter monteringen av tornet ska undergjutning utföras. Undergjutning utförs med ett härför avsett krympningskompenserat specialbruk, exempelvis BEMIX* expanderande köldbrik eller likvärdigt. Undergjutningen ska vara något mindre än fotplattan för att vatten inte ska samlas mellan bruk och fotplatta.

*Finja Bemix AB, Tel 08-594 115 00, www.finjabemix.se

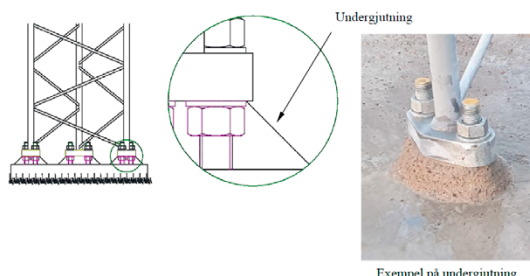


Figure 4-1. A possible cause of seasonal variations in baseline results may be temperature-related expansion in one or more parts of the truss mast. Special attention should be given the three anchor points of the truss mast. A slight difference of 0.1 mm due to thermal expansion in one of the anchor points will result in a horizontal motion at the 1-millimeter level in the top of the mast, at the location of the antenna.



Figure 4-2. Yet another possible cause of seasonal variations in baseline results may be temperature-related changes in the antenna phase center.

4.1 Recommendations for the future

4.1.1 GNSS data analysis software packages and methods

The method called Precise Point Positioning (PPP) is nowadays available in many different software packages such as the Bernese Software (Dach et al. 2015) and GipsyX. It is a very fast and effective method. Processing of one day of data from one station takes about 1 minute on standard type PC. However, in order to achieve results of the highest precision, satellite orbit and clock products at the level of a few centimeters are required. Such products become available from the International GNSS Service (IGS) the day after the actual day of observation.

In order to do near real-time data processing of the SKB stations one has to rely on predicted products from e.g., the IGS. The quality of these satellite orbits and clock products are currently at level of 5 to 10 centimeters and probably not suitable for the monitoring of the SKB stations. Our recommendation is therefore to use either the final or the rapid quality assured products from the IGS when using the PPP method.

To some extent the recommendation is slightly different for software packages simultaneously processing data from a network of stations using single- and double differencing methods (e.g., the Bernese Software). Still high-precision and quality-assured satellite orbits are recommended. However, real-time satellite clocks are not required since the satellite and receiver clocks are cancelled when using double differencing. Thus, the processing can be based on predicted orbits and still give sub-centimeter results, however, perhaps not down to 2–3 millimeters as for the high-quality products from IGS.

In order to monitor station motions, real- or near real-time GNSS data processing is probably not the best method but utilizing e.g., the Bernese Software will result in sub-centimeter coordinates in real time.

Independently from the processing method, PPP or double differencing, the most sophisticated software packages also have the capability to estimate coordinates at any given sampling rate. This means that the PPP results presented in this report could be complemented by the same type of GNSS data analysis but instead of estimating coordinates once per 24 hours we could have set up the Kalman filter to output coordinate estimates e.g., every hour. This could be used in order to study variations within a 24-hour data set. However, the level of uncertainty will grow as the number of estimated parameters increases.

4.1.2 GNSS station hardware

When upgrading or adding new station, make sure to use the state-of-the-art receivers, antennas cable and antennas. The SWEPOS operational centre at Lantmäteriet are continuously evaluating new hardware and keep track of new findings within the community.

New receiving systems should be able to track all GNSS signals. Specific care has to be taken to the antenna type and seeing to that the all antennas are calibrated with and without the plastic cover i.e., radome. Also, the antenna cables are developed and besides the traditional types of coaxial cable many organisations in the GNSS time and frequency community are using optical cables. Anyway, a strong recommendation is to follow the development of SWEPOS when deciding about receivers, antennas and antenna cables. Since all processing should also include the nearest SWEPOS stations as reference stations it is favourable to utilize SWEPOS-consistent station hardware.

The monuments used in SWEPOS today are of many different types. For the core stations we expect results at the very few millimetres level in terms of precision/repeatability. Thus, special care has been taken when selecting and evaluating monument types for these stations.

Access to solid bedrock is one of the requirements. Free horizon around the selected site is very important. Also, foliage and problems with the electromagnetic environment i.e., multipath will degrade the observational conditions. The monument types tested in SWEPOS today are truss (steel grid) masts of different heights (1–4 meters) and/or concrete pillars (1–3 meters) that are temperature controlled.

The latest results show that the multipath (near-field scattering) is less serious when using the truss masts. A one-meter truss mast attached to bed rock using equally long bolts and surrounded by very low vegetation would be the best choice. With a high probability, it is the mast foot and mast top

that are the parts of the mast that can be more sensitive to temperature variations. The installation should follow the SWEPOS recommendation and addition it could be useful to hide the mast foot in Styrofoam. Also, discussion with Lantmäteriet about the top of the mast should be initiated.

4.1.3 Recommended further testing

The data set now contain almost 5 years of daily GNSS-data. Adding almost two years of data to the existing time series in this report would probably help when trying to identify possible error sources. Furthermore, all five years could be re-analyzed with coordinate estimates every second hour in order to find variation of within days. For example, this kind of variations over 24 hours should be correlated with temperature data from Forsmark (or SMHI).

We suggest that an experimental stations, consisting of two three-meter truss mast with a fully equipped receiving system is set up either in Forsmark or at AstaZero. Investigations of the temperature sensitivity of the antenna, antenna cable and the mast itself can be performed in a controlled environment without additional electromagnetic interferences.

References

SKB's (Svensk Kärnbränslehantering AB) publications can be found at www.skb.com/publications.

Bertiger W, Bar-Sever Y E, Dorsey A, Haines B, Harvey N, Hemberger D, Heflin M, Lu W, Miller M, Moore A W, Murphy D, Ries P, Romans L, Sibois A, Sibthorpe A, Szilagyi B, Vallisneri M, Willis P, 2020. GipsyX/RTGx, a new tool set for space geodetic operations and research, *Advances in Space Research* 66:3, 469–489. <https://doi.org/10.1016/j.asr.2020.04.015>

Dach R, Lutz S, Walser P, Fridez P (eds), 2015. Bernese GNSS Software Version 5.2; User Manual. Bern: University of Bern Astronomical Institute: Bern Open Publishing.

Johansson J M, Davis J L, Scherneck H-G, Milne G A, Vermeer M, Mitrovica J X, Bennett R A, Jonsson B, Elgered G, Elósegui P, Koivula H, Poutanen M, Rönnäng B O, Shapiro I I, 2002. Continuous GPS measurements of postglacial adjustment in Fennoscandia 1. Geodetic results. *Journal of Geophysical Research: Solid Earth* 107:B8, ETG 3-1 –ETG 3-27. <https://doi.org/10.1029/2001JB000400>

Kierulf H P, Steffen H, Barletta V R, Lidberg M, Johansson J, Kristiansen O, Tarasov L, 2021. A GNSS velocity field for geophysical applications in Fennoscandia. *Journal of Geodynamics* 146, 101845. <https://doi.org/10.1016/j.jog.2021.101845>

Lidberg M, Johansson J M, Scherneck H G, Davis J L, 2007. An improved and extended GPS-derived 3D velocity field of the glacial isostatic adjustment (GIA) in Fennoscandia. *Journal of Geodesy* 81, 213–230. <https://doi.org/10.1007/s00190-006-0102-4>

Lehner W M, 2011. Evaluation of Environmental Stress on GNSS-monuments. Master Thesis. Vienna University of Technology and Chalmers University of Technology Sweden.

Zumberge J F, Heflin M B, Jefferson D C, Watkins M M, Webb F H, 1997. Precise point positioning for the efficient and robust analysis of GPS data from large networks. *Journal of Geophysical Research: Solid Earth* 102, 5005–5017. <https://doi.org/10.1029/96JB03860>

Deliverables and Data formats

The file delivered with this project are produced by single station process using the method called Precise Point Positioning with the software package GipsyX.

The stacov files

For every day and every station in the network a file containing the coordinate results is produced. The file name convention is *YYYY-MM-DD_10SSSS.stacov*. *YYYY-MM-DD* is the date of the day and the following *10* means that a 10-degree elevation cut-off angle was used. Finally, the *SSSS* gives the four-letter abbreviation of the station name followed by *stacov* pointing out that the file contains the X, Y, Z coordinates estimates for this specific station on this specific day. The coordinates are given in an Earth centred system called ITRF2014. The numbers are given in meters and so are the uncertainties.

```

3 PARAMETERS ON 20DEC02.
1 VMA0 STA X      2.999706623913022e+06 +- 1.014132634221152e-03
2 VMA0 STA Y      9.904963231004283e+05 +- 8.201457345152911e-04
3 VMA0 STA Z      5.522330585386266e+06 +- 1.567107824139255e-03
2   1   1.536784945057695e-01
3   1   7.194233733928885e-01
3   2   3.095792844413806e-01

```

Figure A-1. Example of a stacov file containing the X, Y and Z coordinate results for the station VMA0 on 2020-12-02. The coordinates are given in meters relating to the Earth fixed ITRF2014. Also, the RMS uncertainties are given in meters for each coordinate. The cross correlation between the different coordinate parameters are given in the last three lines.

The .lat, .lon and .rad files

All the daily results from a specific station and found in the stacov files described above are then combined. The resulting files contains the relative change of the station coordinates in a geodetic coordinate system, still in ITRF2014, where the starting point refers to the coordinates of the first day in the combination. There is one file for the latitude (north–south) component, one for the longitude (east–west) component and one for the radial (height) coordinate component. The first column gives the day of data in the unit [Year], the second column shows the relative change of the coordinate since the reference file (starting date of the combination) in meters and the third column gives the RMS uncertainty of the value in column two.

```
2020.90075291 0.028559 0.000611
2020.90349076 0.028916 0.000613
2020.90622861 0.027653 0.000622
2020.90896646 0.028493 0.000621
2020.91170431 0.026778 0.000610
2020.91444216 0.028108 0.000621
2020.91718001 0.028604 0.000618
2020.91991786 0.028222 0.000607
2020.92265572 0.029507 0.000631
2020.92539357 0.030408 0.000622
2020.92813142 0.031323 0.000612
2020.93086927 0.030259 0.000614
2020.93360712 0.029991 0.000621
2020.93634497 0.030192 0.000619
2020.93908282 0.028013 0.000612
2020.94182067 0.030150 0.000621
```

Figure A-2. A part of the file *VMA0_10.lat* is used in order to describe the content and format of the time series result files. The first column contains the time of the results in decimal years. For example, 2020.900 day 329 of the total of 366 days in 2020. The second column gives the relative change in latitude (north–south) of the station coordinates, in meters, with respect to the starting date used in the combination. Finally, the third column contains the RMS uncertainties of the values in column two in meters. As can be seen, the output from GipsyX indicates sub-millimetres quality in the daily results. However, the day-to-day repeatability varies much more. All this are visualized by the plots in this report.

The .env and .ltu files

The files ending with either .env or .ltu contains information about the relative distance between two stations in a vector form. The .env file contains information about the East (e), North (n) and Vertical (v) vectors between the two stations while the .ltu files contain the straight distance between the stations, i.e., length (l). The file also contains the standard deviation for the different parameters as well as covariances between the parameters.

It is important to note that since GipsyX is used in PPP mode, the comparison of the three-dimensional motion between two stations are only possible in post-processing and therefore only utilizes the coordinate results from each day and station. This is different from the results produced by e.g., the network solution with the Bernese Software. In the latter case two or more stations are processed together and the raw observables are combined when the single- and double-differencing are applied. A quick comparison between the GipsyX PPP baseline results reported here with the results from the Bernese Software reported by Lantmäteriet does, however, not indicate a significant difference.

2018.91581109	2365.324317	-1719.000764	-1.954602	0.001041	0.000804	0.002367	0.021043	-0.010534	-0.036127
2018.91854894	2365.325251	-1719.001078	-1.952615	0.001062	0.000825	0.002428	0.041552	-0.007965	0.009841
2018.92128679	2365.327139	-1719.001664	-1.956086	0.001066	0.000821	0.002356	0.026023	-0.004780	-0.034551
2018.92676249	2365.327704	-1719.001481	-1.957486	0.001089	0.000815	0.002440	0.045250	-0.007440	-0.019581
2018.92950034	2365.326851	-1719.001084	-1.956112	0.001064	0.000814	0.002371	0.045277	-0.003306	-0.024223
2018.93223819	2365.326232	-1719.001892	-1.954687	0.001068	0.000813	0.002351	0.053565	-0.012544	-0.034385
2018.93497604	2365.326242	-1719.000408	-1.959043	0.001034	0.000803	0.002380	0.041389	-0.001618	-0.022544
2018.93771309	2365.325991	-1719.000179	-1.952582	0.001058	0.000821	0.002419	0.033125	0.010251	-0.028627
2018.94045175	2365.327373	-1719.002420	-1.954545	0.001066	0.000814	0.002339	0.033881	0.003506	-0.044246
2018.94318960	2365.326831	-1719.001843	-1.956399	0.001038	0.000797	0.002344	0.023172	-0.003514	-0.040636
2018.94592745	2365.327702	-1719.002435	-1.954073	0.001052	0.000802	0.002398	0.020530	-0.008755	-0.015900
2018.94866530	2365.327694	-1719.002072	-1.956156	0.001072	0.000819	0.002359	0.041474	-0.006800	-0.041784

Figure A-3. The .env files as well as the .ltu shows three-dimensional (e.g., East, North and Vertical) distance between two stations. The first column is time in decimal years. Columns 2–4 show the three-dimensional vector (E, N, V) in meters, columns 5–7 the standard deviation in meters, and finally columns 8–10 show the covariances for EN, EV and NV in meters.

SKB is responsible for managing spent nuclear fuel and radioactive waste produced by the Swedish nuclear power plants such that man and the environment are protected in the near and distant future.

skb.se